A POSTERIORI ERROR ESTIMATOR FOR ADAPTIVE LOCAL BASIS FUNCTIONS TO SOLVE KOHN–SHAM DENSITY FUNCTIONAL THEORY*

JASON KAYE†, LIN LIN‡, AND CHAO YANG§

Abstract. Kohn–Sham density functional theory is one of the most widely used electronic structure theories. The recently developed adaptive local basis functions form an accurate and systematically improvable basis set for solving Kohn–Sham density functional theory using discontinuous Galerkin methods, requiring a small number of basis functions per atom. In this paper, we develop residual-based, a posteriori error estimates for the adaptive local basis approach, which can be used to guide non-uniform basis refinement for highly inhomogeneous systems such as surfaces and large molecules. The adaptive local basis functions are non-polynomial basis functions, and standard a posteriori error estimates for hp-refinement using polynomial basis functions do not directly apply. We generalize the error estimates for hp-refinement to non-polynomial basis functions. We demonstrate the practical use of the a posteriori error estimator in performing three-dimensional Kohn–Sham density functional theory calculations for quasi-2D aluminum surfaces and a single-layer graphene oxide system in water.

Key words. Kohn–Sham density functional theory, a posteriori error estimator, adaptive local basis function, discontinuous Galerkin method.

AMS subject classifications. 65N15, 65N25, 65N30, 65Z05.

1. Introduction

In this paper, we consider an a posteriori error estimator of the eigenvalues and eigenvectors of the following linear eigenvalue problem:

$$\left(-\frac{1}{2}\Delta + V\right)\psi_i = \varepsilon_i \psi_i,$$
$$\int \psi_i^*(\mathbf{r})\psi_j(\mathbf{r})\,\mathrm{d}\mathbf{r} = \delta_{ij}, \quad i,j = 1,\dots,N, \tag{1.1}$$

where $\{\psi_i\}_{i=1}^N$ are the eigenvectors corresponding to the lowest N eigenvalues $\{\varepsilon_i\}_{i=1}^N$. This problem arises in solving the Kohn–Sham nonlinear eigenvalue problem

$$H[\rho]\psi_i = \varepsilon_i \psi_i,$$
$$\rho(\mathbf{r}) = \sum_{i=1}^N |\psi_i(\mathbf{r})|^2, \quad \int \psi_i^*(\mathbf{r})\psi_j(\mathbf{r})\,\mathrm{d}\mathbf{r} = \delta_{ij}, \tag{1.2}$$

where N is the number of electrons (spin degeneracy is omitted here for simplicity), $\{\varepsilon_i\}_{i=1}^N$ are the Kohn–Sham eigenvalues, and $\{\psi_i\}_{i=1}^N$ are called the Kohn–Sham eigenfunctions or orbitals. These eigenfunctions define the electron density $\rho(\mathbf{r})$, which in turn defines the Kohn–Sham Hamiltonian

$$H[\rho] = -\frac{1}{2}\Delta + V_{\mathrm{hxc}}[\rho] + V_{\mathrm{ion}}, \tag{1.3}$$

†Courant Institute of Mathematical Sciences, New York University, New York, NY 10012, USA (jkaye@cims.nyu.edu).

‡Department of Mathematics, University of California, Berkeley and Computational Research Division, Lawrence Berkeley National Laboratory, Berkeley, CA 94720, USA (linlin@math.berkeley.edu).

§Computational Research Division, Lawrence Berkeley National Laboratory, Berkeley, CA 94720, USA (cyang@lbl.gov).

where Δ is the Laplacian operator for characterizing the kinetic energy of electrons, $V_{\mathrm{hxc}}[\rho]$ is a nonlinear function of ρ which includes the electro-static interaction (Hartree) potential among electrons (h) and the exchange-correlation potential (xc), and V_{ion} is the electron-ion interaction potential, which is independent of ρ. We denote by Ω the global computational domain, and for simplicity we assume each eigenfunction ψ_i has periodic boundary conditions on Ω. This nonlinear eigenvalue problem is the key problem to be solved in the Kohn–Sham density functional theory (KSDFT) [22, 26], which is the most widely used electronic structure theory for studying properties of molecules, solids, and other nano structures.

Since the eigenvalue problem (1.2) is nonlinear, it is often solved iteratively by a class of algorithms called *self-consistent field iterations* (SCF) [30]. At each SCF step, a linear eigenvalue problem with a fixed Kohn–Sham Hamiltonian defined by a fixed electron density ρ (1.3) is solved. The solution to this linear eigenvalue problem is used to update ρ and H in the SCF iteration. Solving (1.3) is the most computationally expensive part of the SCF iteration. Although the asymptotic complexity of the computation with respect to the number of atoms depends on the algorithm used to solve the algebraic eigenvalue problem, the prefactor, which is related to the number of basis functions per atom, is characterized by how the problem is discretized. In this paper, we consider a discretization scheme in which an eigenfunction of $H[\rho]$ is expressed as a linear combination of basis functions that have localized nonzero support. The use of these localized basis functions yields a compact and yet sparse representation of the Kohn–Sham Hamiltonian so that a relatively small prefactor in SCF iteration complexity can be achieved.

The generation of localized basis functions for discretizing the Kohn–Sham problem is described in [28]. The basic idea is to partition the global domain into a number of subdomains (called elements) and solve the Kohn–Sham problem locally around each element to generate local basis functions. The constructed basis functions are not continuous across the boundaries of different elements. Therefore, we use the discontinuous Galerkin (DG) method to construct a finite dimensional Kohn–Sham Hamiltonian represented by these types of discontinuous basis functions.

Furthermore, these basis functions are modified in each SCF cycle as the electron density ρ, and consequently, the Kohn–Sham Hamiltonian is changed. Hence these basis functions are called adaptive local basis functions (ALB) because they adapt to the changes in ρ and $H[\rho]$, which include all the information of the atomic configuration and the electronic structure. The use of ALB combines the systematically improvable standard discretization methods such as the planewave method [33], the finite difference method [9], and the finite element method [40] with a small number of degrees of freedom of "mesh free" basis sets such as numerical atomic orbitals and Gaussian type orbitals [31, 6, 24, 11, 1, 35].

We have already demonstrated the effectiveness of ALB for spatially homogeneous systems such as disordered bulk Na and Si systems studied in [28]. For these systems, the same number of local basis functions are constructed in each element. For inhomogeneous systems, such as large molecules and surfaces systems, there are usually large vacuum regions in the computational domain. It is conceivable that one does not need to compute too many eigenfunctions of the Kohn–Sham Hamiltonian restricted to these regions to generate the adaptive local basis functions. By reducing the number of basis functions generated from these regions, we can reduce the total number of basis functions. In this paper, we develop an adaptive refinement strategy which allows different numbers of localized basis functions to be generated on different elements. The

decision of how many basis functions to generate on each element will be guided by an *a posteriori* error estimator. We demonstrate that the resulting non-uniform generation of ALB functions is highly efficient for KSDFT calculations on inhomogeneous systems.

A posteriori error estimates for solutions to elliptic partial differential equations (PDEs) using DG methods have been established in [23, 25, 37]. The authors considered error estimation for polynomial basis functions in the context of both h-refinement and hp-refinement. The most relevant work to our study appeared recently for the eigenvalue problem of the Laplacian operator [19]. Recent work in applying DG hp-refinement to solve eigenvalue problems arising from the analysis of photonic crystals can be found in [18]. The a posteriori error estimator proposed in [19] is residual-based. Alternative approaches based on flux reconstruction have also been proposed [7, 17, 29, 36]. The key tool used in the analysis in [19] is the decomposition of the discontinuous solution to an eigenvalue problem into an H^1 component in the global domain (the conforming part) and a remaining component (the non-conforming part). The construction of the a posteriori error estimator depends explicitly on the analytic properties of the broken polynomial space used in hp-refinement. This type of technique cannot be directly applied to non-polynomial basis functions such as ALBs for the Kohn–Sham problem.

We also acknowledge that the use of a posteriori error estimates for solving eigenvalue problems discretized with a continuous basis set has also been largely investigated, see e.g. Refs. [41, 5, 27, 16]. Recently, adaptive refinement in KSDFT calculations has also been proposed in the context of the finite element method [15, 10] and the finite volume method [14].

The contribution of this paper is twofold: 1) We illustrate the theory of residual-based a posteriori error estimates for solving linear eigenvalue problems using non-polynomial basis functions, and 2) We present numerical results of using the residual-based a posteriori error estimates to solve the nonlinear Kohn–Sham equations efficiently. From a theoretical point of view, we use the same strategy as that employed in [19] to develop residual-based a posteriori error estimates for solving KSDFT using ALBs. Besides the Laplacian term, our estimator takes into account the presence of a non-constant potential term as required in KSDFT. To address the lack of analytical expressions for the basis functions, we propose a set of assumptions on the function space spanned by a basis set which would render the resulting a posteriori error estimator an upper bound for the errors of both eigenvalues and eigenvectors, up to terms which are of higher order in the context of standard hp-refinement. The main limitation of the current approach is that it is difficult to directly verify the postulated assumptions for a specific non-polynomial basis set, such as the ALBs, since the a priori error analysis of ALBs is not yet available. This also makes it difficult to verify that the neglected terms are indeed of higher order than the estimator and to prove that the estimator also gives a lower bound for the errors of eigenvalues and eigenvectors.

From a numerical point of view, the results are encouraging. As a first attempt to apply our analysis to practical calculations, we use the same form of a posteriori error estimator as that given in [19] but reinterpret p as the number of ALBs rather than the polynomial degree. The numerical results from 3D KSDFT calculations indicate that the a posteriori error estimator captures the spatial inhomogeneity of the system and therefore gives a promising approach to improving the accuracy of solutions to KSDFT without increasing the computational cost.

The rest of the manuscript is organized as follows. In Section 2, we introduce the DG framework for solving KSDFT and the construction of the ALBs. Section 3 is devoted to the derivation of the residual-based a posteriori error estimator for the ALBs,

as well as an explanation of the non-uniform refinement strategy. The effectiveness of the non-uniform refinement strategy is verified in Section 4 by applying the refinement strategy to the solution of the Kohn–Sham problem for a quasi-2D aluminum surface and a 3D graphene oxide in water system. The conclusion and discussion of future work on refining the a posteriori error estimator are given in Section 5. The details of the proofs used in Section 3 are provided in the appendix.

2. Preliminaries

2.1. Discontinuous Galerkin framework for KSDFT.   In a standard Galerkin method, we seek the solution to the Kohn–Sham nonlinear eigenvalue problem by working with its weak form

$$\langle v, H[\rho]u_i \rangle_\Omega = \varepsilon_i \langle v, u_i \rangle_\Omega, \tag{2.1}$$

where $\langle \cdot, \cdot \rangle_\Omega$ is an appropriately chosen inner product defined on the global domain Ω, which is assumed throughout this paper to be a d-dimensional rectangular domain, and v is a test function. To comply with standard notation in the DG analysis, we use $u_i(\mathbf{r}) \equiv \psi_i(\mathbf{r})$ to represent the ith Kohn–Sham orbital corresponding to the eigenvalue ε_i.

For example, we may choose $\langle \cdot, \cdot \rangle_\Omega$ to be the standard L_2 inner product

$$\langle u, v \rangle_\Omega = \int_\Omega u^*(\mathbf{r})v(\mathbf{r})\,\mathrm{d}\mathbf{r}, \tag{2.2}$$

with the induced norm $\|\cdot\|$ defined by

$$\|u\|_\Omega = \langle u, u \rangle_\Omega^{\frac{1}{2}}.$$

Both the approximate eigenfunctions u_i and the test function v must be chosen from an appropriate function space so that the weak form (2.1) is well defined. For example, if we let $L^2(\Omega)$ be the space of square integrable functions on Ω, and $H^1(\Omega)$ be the space of functions in $L^2(\Omega)$ with gradient in $[L^2(\Omega)]^d$, then u_i and v can be chosen from $H^1_\pi(\Omega)$, the subspace of $H^1(\Omega)$ functions with periodic boundary conditions.

Although KSDFT is formulated as a nonlinear eigenvalue problem, the a posteriori error estimator developed in this paper is for a linear eigenvalue problem, with the linear Hamiltonian operator obtained from each step of the SCF iteration. For a fixed ρ we define an effective potential

$$V_{\mathrm{eff}}[\rho] = V_{\mathrm{hxc}}[\rho] + V_{\mathrm{ion}}. \tag{2.3}$$

We note that $V_{\mathrm{eff}}[\rho]$ defines an effective Hamiltonian operator $H_{\mathrm{eff}}[\rho] = -\frac{1}{2}\Delta + V_{\mathrm{eff}}[\rho]$. For brevity, we will omit the dependence on ρ. The effective Kohn–Sham potential V_{eff} is, in general, a symmetric operator, and thus satisfies

$$\langle u, V_{\mathrm{eff}}v \rangle_\Omega = \langle V_{\mathrm{eff}}u, v \rangle_\Omega, \quad \forall u, v \in H^1_\pi(\Omega). \tag{2.4}$$

When V_{ion} is constructed using the pseudopotential method [39], V_{eff} is bounded from above and from below thereby ensuring that (2.1) is indeed well defined when $u_i, v \in H^1_\pi(\Omega)$.

Among the various Galerkin methods, the discontinuous Galerkin (DG) methods relax the continuity constraint on basis functions and provide flexibility in choosing the basis set. For instance, the adaptive local basis functions are given by solutions

to Kohn–Sham problems on local subdomains and are naturally discontinuous in the global domain. The DG methods have been developed to efficiently solve various types of PDEs, and there is an abundant literature about them; see [4, 43, 2, 12, 13, 3, 38]. In the ALB approach [28], the interior penalty (IP) method [4, 2] is used to discretize the Kohn–Sham Hamiltonian operator.

We assume that the d-dimensional rectangular global domain Ω is partitioned into a collection of uniform rectangular subdomains, denoted by

$$\mathcal{T} = \{K_1, K_2, \cdots, K_M\}. \tag{2.5}$$

Each subdomain $K_i \in \mathcal{T}$ is called an element of Ω. Associated with each K_i is an inner product $\langle \cdot, \cdot \rangle_{K_i}$ defined by simply replacing Ω in (2.2) with K_i. The induced norm of a function u defined on K_i is denoted by $\|u\|_{K_i} \equiv \langle u, u \rangle_{K_i}^{1/2}$.

We refer to F as a face of $\mathcal{T}$ if $F \subset \partial K$ is a face of the d-dimensional rectangular subdomain $K \in \mathcal{T}$. We refer to F as an interior face of $\mathcal{T}$ if $F = \partial K^+ \cap \partial K^-$ for some neighboring elements $K^+, K^- \in \mathcal{T}$. We note that when using periodic boundary conditions all faces are interior faces. Other types of boundary conditions, such as Dirichlet boundary conditions, can be used as well, and the discussion below can be naturally generalized to cases with boundary faces.

In the DG framework, u_i is constructed as a linear combination of M local basis functions that form a subspace from which v is drawn. Because each basis function has support contained in one of the elements and is not necessarily continuous over the entire domain Ω, an appropriate inner product should be chosen to make the weak form (2.1) well defined.

To define such an inner product, let us first define the discontinuous function spaces

$$\mathcal{V}(\mathcal{T}) = \{v \in L^2(\Omega) : v|_K \in H^1(K),\ K \in \mathcal{T}\}. \tag{2.6}$$

The inner product associated with $\mathcal{V}(\mathcal{T})$ is

$$\langle u, v \rangle_{\mathcal{T}} = \sum_{K \in \mathcal{T}} \langle u, v \rangle_K \equiv \sum_{K \in \mathcal{T}} \int_K u^*(\mathbf{r}) v(\mathbf{r})\, d\mathbf{r}, \quad u, v \in \mathcal{V}(\mathcal{T}). \tag{2.7}$$

We denote by $\mathcal{S}$ the collection of all the faces $\{F\}$. An inner product associated with functions defined on $\mathcal{S}$ is

$$\langle u, v \rangle_{\mathcal{S}} = \sum_{F \in \mathcal{S}} \langle u, v \rangle_F \equiv \sum_{F \in \mathcal{S}} \int_F u^*(\mathbf{r}) v(\mathbf{r})\, ds(\mathbf{r}). \tag{2.8}$$

The gradient of a function defined on K has d components. A natural inner product for this type of vector function space is

$$\langle \mathbf{q}, \mathbf{w} \rangle_K = \int_K \mathbf{q}^*(\mathbf{r}) \cdot \mathbf{w}(\mathbf{r})\, d\mathbf{r}, \tag{2.9}$$

for $\mathbf{q}, \mathbf{w} \in [L^2(K)]^d$.

If we define the vector function space $\mathcal{W}(\mathcal{T}) \equiv [L^2(\Omega)]^d$, then

$$\langle \mathbf{q}, \mathbf{w} \rangle_{\mathcal{T}} = \sum_{K \in \mathcal{T}} \langle \mathbf{q}, \mathbf{w} \rangle_K \equiv \sum_{K \in \mathcal{T}} \int_K \mathbf{q}^*(\mathbf{r}) \cdot \mathbf{w}(\mathbf{r})\, d\mathbf{r}, \quad \mathbf{q}, \mathbf{w} \in \mathcal{W}(\mathcal{T}) \tag{2.10}$$

is a natural inner product associated with $\mathcal{W}(\mathcal{T})$.

Similarly, we can define an inner product for vector functions defined only on the collection of faces $\mathcal{S}$, i.e.

$$\langle \mathbf{q}, \mathbf{w} \rangle_{\mathcal{S}} = \sum_{F \in \mathcal{S}} \langle \mathbf{q}, \mathbf{w} \rangle_F \equiv \sum_{F \in \mathcal{S}} \int_F \mathbf{q}^*(\mathbf{r}) \cdot \mathbf{w}(\mathbf{r}) \, ds(\mathbf{r}). \tag{2.11}$$

The inner products defined by (2.7), (2.8), (2.10), and (2.11) induce the following norms:

$$\|u\|_{\mathcal{T}}^2 = \langle u, u \rangle_{\mathcal{T}}, \quad \|u\|_{\mathcal{S}}^2 = \langle u, u \rangle_{\mathcal{S}}, \quad \|\mathbf{q}\|_{\mathcal{T}}^2 = \langle \mathbf{q}, \mathbf{q} \rangle_{\mathcal{T}}, \quad \|\mathbf{q}\|_{\mathcal{S}}^2 = \langle \mathbf{q}, \mathbf{q} \rangle_{\mathcal{S}}. \tag{2.12}$$

If u_i and v are chosen from $H_\pi^1(\Omega)$ in a standard Galerkin method, the weak form (2.1) can be written as

$$A(u_i, v) + \langle V_{\text{eff}} u_i, v \rangle_\Omega = \varepsilon_i \langle u_i, v \rangle_\Omega, \tag{2.13}$$

where the bilinear form $A(u, v)$ is defined by

$$A(u, v) \equiv \frac{1}{2} \langle \nabla u, \nabla v \rangle_\Omega, \tag{2.14}$$

and the eigenfunctions are orthonormal; i.e., $\langle u_i, u_j \rangle = \delta_{i,j}$.

In a DG approach, when u_i and v are chosen from $\mathcal{V}(\mathcal{T})$, the bilinear form $A(u_i, v)$ includes $\frac{1}{2} \langle \nabla u_i, \nabla v \rangle_{\mathcal{T}}$ and some additional terms that account for the discontinuity of the basis functions. To define these terms, let K^+ and K^- be two adjacent elements in $\mathcal{T}$, and let $F = \partial K^+ \cap \partial K^-$ be the face shared by K^+ and K^-. The normal vectors on F are defined to be $\mathbf{n}^+$ and $\mathbf{n}^-$ and point towards the exteriors of K^+ and K^-, respectively. Let $v^+ = v|_{K^+}$, $v^- = v|_{K^-}$, $\mathbf{q}^+ = \mathbf{q}|_{K^+}$ and $\mathbf{q}^- = \mathbf{q}|_{K^-}$. Then the average operator $\{\{\cdot\}\}$ on F is defined by

$$\{\{v\}\} = \tfrac{1}{2}(v^+ + v^-), \quad \text{on } F, \qquad \{\{\mathbf{q}\}\} = \tfrac{1}{2}(\mathbf{q}^+ + \mathbf{q}^-), \quad \text{on } F. \tag{2.15}$$

We define the jump operator $[\![\cdot]\!]$ on F by

$$[\![v]\!] = v^+ \mathbf{n}^+ + v^- \mathbf{n}^-, \quad \text{on } F, \qquad [\![\mathbf{q}]\!] = \mathbf{q}^+ \cdot \mathbf{n}^+ + \mathbf{q}^- \cdot \mathbf{n}^-, \quad \text{on } F. \tag{2.16}$$

To derive a finite dimensional representation of the weak form (2.13), let us assume that we have chosen for each element K a set of orthonormal basis functions $\{\varphi_{K,j}\}_{j=1}^{J_K}$ where $\varphi_{K,j} \in H^1(K)$ and J_K is the number of basis functions in K. The collection of basis functions for each element is denoted by $\mathcal{J} = \{J_1, \cdots, J_M\}$ where M is the total number of elements. We extend each $\varphi_{K,j}$ to the whole computational domain Ω by setting it to 0 on $\Omega \backslash K$. Then the function space $\mathcal{V}_{\mathcal{J}}(\mathcal{T})$, which is a subspace of $\mathcal{V}(\mathcal{T})$ used to approximate each u_i, is defined as

$$\mathcal{V}_{\mathcal{J}}(\mathcal{T}) = \text{span}\{\varphi_{K,j}, K \in \mathcal{T}, j = 1, \ldots, J_K\}. \tag{2.17}$$

For reasons that will be made clear in subsequent analysis, we assume that any function that is piecewise constant over element boundaries is in $\mathcal{V}_{\mathcal{J}}(\mathcal{T})$; i.e.,

$$\mathbf{1}_K \in \text{span}\{\varphi_{K,j}\}_{j=1}^{J_K}, \quad \text{for all } K \in \mathcal{T}, \tag{2.18}$$

where $\mathbf{1}_K$ denotes the characteristic function on K.

A particular example of $\mathcal{V}_{\mathcal{J}}(\mathcal{T})$ is the *broken polynomial space* which takes $\varphi_{K,j}$ to be a polynomial on K. A broken polynomial space is said to be of order p if $\{\varphi_{K,j}\}_{j=1}^{J_K}$ restricted to K consists of polynomials of degree up to p.

The derivative space associated with $\mathcal{V}_{\mathcal{J}}(\mathcal{T})$ is defined as

$$\mathcal{W}_{\mathcal{J}}(\mathcal{T}) = \mathrm{span}\{\nabla\varphi_{K,j}, K \in \mathcal{T}, j = 1, \ldots, J_K\}. \tag{2.19}$$

It is clear that $\mathcal{W}_{\mathcal{J}}(\mathcal{T}) \subset \mathcal{W}(\mathcal{T})$. It is worth noting that in the broken polynomial case each component in the derivative space $\partial_i\varphi_{K,j}$, $i = 1, \ldots, d$ is a polynomial of lower order and therefore is in the function space $\mathcal{V}_{\mathcal{J}}(\mathcal{T})$. However, this property does not hold for general basis sets, so that the functions in $\mathcal{V}_{\mathcal{J}}(\mathcal{T})$ and the components of the functions in $\mathcal{W}_{\mathcal{J}}(\mathcal{T})$ may belong to different function spaces.

Given the function space $\mathcal{V}_{\mathcal{J}}(\mathcal{T})$, we formulate the eigenvalue problem (2.13) in the discontinuous Galerkin framework using the interior penalty method described in [2]. Namely, we seek the first N approximate eigenpairs $(\varepsilon_{i,\mathcal{J}}, u_{i,\mathcal{J}}) \in \mathbb{R} \times \mathcal{V}_{\mathcal{J}}(\mathcal{T})$ such that

$$A_{\mathcal{J}}(u_{i,\mathcal{J}}, v_{\mathcal{J}}) + \langle V_{\mathrm{eff}} u_{i,\mathcal{J}}, v_{\mathcal{J}}\rangle_{\mathcal{T}} = \varepsilon_{i,\mathcal{J}}\langle u_{i,\mathcal{J}}, v_{\mathcal{J}}\rangle, \quad \forall v_{\mathcal{J}} \in \mathcal{V}_{\mathcal{J}}(\mathcal{T}), \tag{2.20}$$

and $\langle u_{i,\mathcal{J}}, u_{j,\mathcal{J}}\rangle_{\mathcal{T}} = \delta_{ij}$. Here, for $u_{\mathcal{J}}, v_{\mathcal{J}} \in \mathcal{V}_{\mathcal{J}}(\mathcal{T})$, the bilinear form $A_{\mathcal{J}}(u_{\mathcal{J}}, v_{\mathcal{J}})$ is given by

$$\begin{aligned} A_{\mathcal{J}}(u_{\mathcal{J}}, v_{\mathcal{J}}) = &\frac{1}{2}\langle \nabla u_{\mathcal{J}}, \nabla v_{\mathcal{J}}\rangle_{\mathcal{T}} - \frac{1}{2}\langle \{\!\{\nabla u_{\mathcal{J}}\}\!\}, [\![v_{\mathcal{J}}]\!]\rangle_{\mathcal{S}} - \frac{1}{2}\langle \{\!\{\nabla v_{\mathcal{J}}\}\!\}, [\![u_{\mathcal{J}}]\!]\rangle_{\mathcal{S}} \\ &+ \sum_{F \in \mathcal{S}} \alpha(J_F)\langle [\![u_{\mathcal{J}}]\!], [\![v_{\mathcal{J}}]\!]\rangle_F, \end{aligned} \tag{2.21}$$

where $\alpha(J_F)$ denotes the interior penalty parameter on the face F which remains to be determined. This parameter penalizes discontinuities of functions across element faces. The values $\{\alpha(J_F)\}$ must be large enough to guarantee that the bilinear form $A_{\mathcal{J}}$ is coercive on $\mathcal{V}_{\mathcal{J}}$. We provide one sufficient condition on $\alpha(J_F)$ for general non-polynomial basis functions in Equation (A.38) and in Corollary A.7.

An alternative way to define $\alpha(J_F)$, which is used in this paper, is to first define a penalty parameter $\alpha(J_K)$ for each element $K \in \mathcal{T}$. Then for each face $F = \partial K^+ \cap \partial K^-$, we define

$$\alpha(J_F) \equiv \max\{\alpha(J_{K^+}), \alpha(J_{K^-})\}. \tag{2.22}$$

Again $\{\alpha(J_K)\}$ should be chosen such that $A_{\mathcal{J}}$ is coercive on $\mathcal{V}_{\mathcal{J}}$.

REMARK 2.1.   In the context of standard hp-refinement, let h_K be the diameter of the element K, and let p_K be highest degree of the polynomials used in K. Then the choice

$$\alpha(p_K) = \frac{\gamma p_K^2}{h_K} \tag{2.23}$$

leads to a coercive bilinear form $A_{\mathcal{J}}$ for a sufficiently large positive value of γ which is independent of p_K and h_K [2, 3]. The choice of γ is in general system-dependent. Condition (A.38) generalizes Equation (2.23).

To solve Equation (2.20) numerically, we write

$$u_{i,\mathcal{J}} = \sum_{K \in \mathcal{T}}\sum_{j=1}^{J_K} c_{K,j;i}\varphi_{K,j}. \tag{2.24}$$

By choosing $v_{\mathcal{J}} = \varphi_{K',j'}$, we turn Equation (2.20) into the following matrix eigenvalue problem:

$$\sum_{K,j} H^{\mathrm{DG}}_{K,j;K',j'} c_{K,j;i} = \varepsilon_{i,\mathcal{J}} c_{K',j';i}, \qquad (2.25)$$

where the matrix elements for the DG Hamiltonian operator are given by

$$H^{\mathrm{DG}}_{K,j;K',j'} = A_{\mathcal{J}}(\varphi_{K,j}, \varphi_{K',j'}) + \langle V_{\mathrm{eff}} \varphi_{K,j}, \varphi_{K',j'} \rangle_{\mathcal{T}}. \qquad (2.26)$$

Since we choose the basis functions to be orthonormal, (2.25) is a standard eigenvalue problem. Because the basis functions have local support, the DG Hamiltonian matrix (2.26) is a sparse matrix, and its eigenvalues and eigenvectors can be computed efficiently on high performance computers.

2.2. Adaptive local basis functions. The local basis functions $\{\varphi_{K,j}\}_{j=1}^{J_K}$ which we use to discretize the Kohn–Sham problem are constructed as follows. For each $K \in \mathcal{T}$, we introduce an associated *extended element* $Q_K \supset K$ with $Q_K \backslash K$ a buffer region surrounding K. We define $V^{Q_K}_{\mathrm{eff}} = V_{\mathrm{eff}}|_{Q_K}$ to be the restriction of the effective potential at the current SCF step to Q_K and solve the local eigenvalue problem

$$\begin{aligned}
\left(-\frac{1}{2}\Delta + V^{Q_K}_{\mathrm{eff}} \right) \widetilde{\varphi}_{K,j} &= \lambda_{K,j} \widetilde{\varphi}_{K,j}, \\
\int_{Q_K} \widetilde{\varphi}^*_{K,j}(\mathbf{r}) \widetilde{\varphi}_{K,j'}(\mathbf{r}) \, d\mathbf{r} &= \delta_{jj'}.
\end{aligned} \qquad (2.27)$$

The lowest J_K eigenvalues $\{\lambda_{K,j}\}_{j=1}^{J_K}$ and the corresponding eigenfunctions $\{\widetilde{\varphi}_{K,j}\}_{j=1}^{J_K}$ are computed. We then restrict $\{\widetilde{\varphi}_{K,j}\}_{j=1}^{J_K}$ from Q_K to K. The truncated vectors are not necessarily orthonormal. Therefore, we apply a singular value decomposition (SVD) to the set of truncated eigenvectors to obtain $\{\varphi_{K,j}\}_{j=1}^{J_K}$. We then set each $\varphi_{K,j}$ equal to zero outside of K, so that it is in general discontinuous across the boundary of K.

There are a number of possible ways to set the boundary conditions for the local problem (2.27). In practice, we use either Dirichlet or periodic boundary conditions for all of the eigenfunctions $\{\widetilde{\varphi}_{K,j}\}_{j=1}^{J_K}$ in Q_K. It is not yet clear what are the optimal boundary conditions. Our ultimate goal is not to solve (2.27), but to use the approximate solution of (2.27) to construct localized basis functions, and any choice of boundary conditions that guarantees $\left(-\frac{1}{2}\Delta + V^{Q_K}_{\mathrm{eff}} \right)$ to be a self adjoint operator on Q_K will generate a complete basis set on K. In this sense, the choice of boundary conditions is not critical for the purposes of this paper. The size of each extended element should be large enough to capture the effect of the chemical environment, but should not be so large that it makes the local problem costly to solve.

We solve the local eigenvalue problem (2.27) using a planewave discretization scheme. It should be noted that the use of a finite dimensional discretization for solving Equation (2.27) would introduce additional error on top of that incurred by using a finite number of adaptive local basis functions in each element. Numerical results indicate that inaccurately solved adaptive local basis functions are less effective in solving the Kohn–Sham equations. In our numerical results, we always use a sufficiently fine planewave discretization to ensure that the error caused by the planewave discretization is negligible compared to the error introduced by the use of a finite number of adaptive local basis functions. We find that the energy cutoff of such planewave discretizations

is comparable to or slightly larger than the energy cutoff of converged calculations obtained from standard electronic structure software packages such as ABINIT.

For a typical choice of grid used in practice, the elements are chosen to be of the same size. Numerical results indicate that it is most efficient if each element contains, on average, a few atoms. The grid does not need to be updated even if the atomic configuration is changed, as in the case of structure optimization and molecular dynamics. Dangling bonds may form when atoms are present on the faces of the extended elements, but we emphasize that these dangling bonds do not need to be passivated by introducing auxiliary atoms near the faces of the extended elements [44]. This is because the potential is not obtained self-consistently within the extended element Q_K, but instead from the restriction of the screened potential in the global domain Ω to Q_K in each SCF iteration which mutes the catastrophic damage of the dangling bonds. On the other hand, one can still introduce auxiliary atoms near the faces of the extended elements, as in the quantum mechanics/molecular mechanics (QM/MM) [42] approach, to achieve a better approximation of the exact boundary conditions for $\widetilde{\varphi}_{K,j}$ than the Dirichlet or periodic boundary condition used here. This is beyond the scope of this manuscript but can be explored in future work.

3. Residual-based a posteriori error estimator

In this section, we develop a posteriori error estimates for ALB sets. Although ALB sets are constructed from solutions to the Kohn–Sham equations restricted to local domains, so far, little can be derived analytically in order to obtain the approximation properties of the function space spanned by the ALBs. Therefore, we do not restrict our scope to ALBs but attempt to directly develop a posteriori error estimates for general non-polynomial basis sets. In the ALB method, the size of each element is usually chosen to include one or several atoms (usually less than 10 per element) to balance efficiency and accuracy. These basis functions are not scale invariant, and the meaning of h-refinement is not straightforward. Therefore, we do not consider h-refinement here, and the number of elements M is fixed. We only consider the refinement of the number of basis functions J_K in each element $K \in \mathcal{T}$. This is analogous to p-refinement.

3.1. Theory. In order to address the apparent difficulty associated with the analysis of general non-polynomial basis sets, we need a set of assumptions on the function space spanned by the ALB functions. These assumptions directly generalize the results in [19] for polynomial basis functions. However, we acknowledge that the assumptions are not easy to verify directly for a given specific basis set such as the ALB set. We will defer the detailed verification of these assumptions for the ALB set to our future work and focus in this paper on the type of error estimates we can obtain and use to adaptively refine the basis set if these assumptions hold. In the following discussion, "$a \lesssim b$" is taken to mean that "a is less than or equal to b up to a constant scaling". The scaling factor a/b depends on the dimensionality d, the total number of elements M, the size of each element K, and the size of the global domain Ω. In particular, the constant is independent of the number of basis functions J_K for each $K \in \mathcal{T}$.

ASSUMPTION 3.1.
  1. (Approximation properties) For any $u \in H^1_\pi(\Omega)$, there exists a function $u_\mathcal{J} \in \mathcal{V}_\mathcal{J}(\mathcal{T})$ such that for each $K \in \mathcal{T}$

$$\|u - u_\mathcal{J}\|^2_K \lesssim \gamma_1(J_K) \|\nabla u\|^2_K, \qquad (3.1)$$

$$\|u - u_\mathcal{J}\|^2_{\partial K} \lesssim \gamma_2(J_K) \|\nabla u\|^2_K, \qquad (3.2)$$

$$\|\nabla(u - u_\mathcal{J})\|^2_K \lesssim \|\nabla u\|^2_K, \qquad (3.3)$$

where the constants γ_1 and γ_2 depend only on J_K. For a given $\mathcal{J} = \{J_1, \cdots, J_M\}$, we define $\gamma_{1,\mathcal{J}} = \max_{K \in \mathcal{T}} \gamma_1(J_K)$. Furthermore, $\gamma_1(\cdot)$ and $\gamma_2(\cdot)$ are bounded from above. The parameter γ_2 satisfies

$$1 \lesssim \gamma_2(J_K) \alpha(J_K). \tag{3.4}$$

2. *(Interpolation properties) There exists an interpolation operator*
   $I_{\mathcal{J}} : \mathcal{V}_{\mathcal{J}}(\mathcal{T}) \to H^1_\pi(\Omega)$ *such that for any* $u_{\mathcal{J}} \in \mathcal{V}_{\mathcal{J}}(\mathcal{T})$

$$\sum_{K \in \mathcal{T}} \|\nabla(u_{\mathcal{J}} - I_{\mathcal{J}} u_{\mathcal{J}})\|^2_K \lesssim \sum_{F \in \mathcal{S}} \gamma_2(J_F) \alpha^2(J_F) \|[\![u_{\mathcal{J}}]\!]\|^2_F. \tag{3.5}$$

Here, for $F = \partial K^+ \cap \partial K^-$, *we write*

$$\gamma_2(J_F) \equiv \max\{\gamma_2(J_{K^+}), \gamma_2(J_{K^-})\}, \quad \alpha(J_F) \equiv \max\{\alpha(J_{K^+}), \alpha(J_{K^-})\}.$$

3. *(Inverse trace inequalities)* $\forall u_{\mathcal{J}} \in \mathcal{V}_{\mathcal{J}}(\mathcal{T})$,

$$\|u_{\mathcal{J}}\|^2_{\partial K} \lesssim \gamma_2(J_K) \alpha^2(J_K) \|u_{\mathcal{J}}\|^2_K, \quad \|\nabla u_{\mathcal{J}}\|^2_{\partial K} \lesssim \gamma_2(J_K) \alpha^2(J_K) \|\nabla u_{\mathcal{J}}\|^2_K. \tag{3.6}$$

The constants in the estimates (3.1) and (3.2) are important components of the a posteriori error estimator. For each element K, we define the local estimator $\eta_{i,K}$ for estimating the error of the ith eigenpair $(\varepsilon_{i,\mathcal{J}}, u_{i,\mathcal{J}})$ as

$$\eta^2_{i,K} = \eta^2_{i,R_K} + \eta^2_{i,G_K} + \eta^2_{i,V_K} \tag{3.7}$$

where

$$\eta^2_{i,R_K} = \gamma_1(J_K) \left\| \left(-\frac{1}{2}\Delta + V_{\text{eff}} - \varepsilon_{i,\mathcal{J}} \right) u_{i,\mathcal{J}} \right\|^2_K, \tag{3.8}$$

$$\eta^2_{i,G_K} = \frac{1}{4} \sum_{F \subset \partial K} \gamma_2(J_F) \|[\![\nabla u_{i,\mathcal{J}}]\!]\|^2_F, \tag{3.9}$$

$$\eta^2_{i,V_K} = \frac{1}{4} \sum_{F \subset \partial K} \gamma_2(J_F) \alpha^2(J_F) \|[\![u_{i,\mathcal{J}}]\!]\|^2_F. \tag{3.10}$$

Here η_{i,R_K} measures the residual (R) of the ith computed eigenfunction on the interior of K, η_{i,G_K} measures the discontinuity of the gradient (G) of the ith computed eigenfunction over the faces of K, and η_{i,V_K} measures the discontinuity of the value (V) of the ith computed eigenfunction over the faces of K. The factor $\frac{1}{4}$ in η_{i,G_K} and η_{i,V_K} comes from the $\frac{1}{2}$ in front of the Laplacian operator in Equation (1.3), as well as the double counting of face terms, by replacing $\sum_{F \in \mathcal{S}}$ with $\sum_{K \in \mathcal{T}} \sum_{F \subset \partial K}$. The notation $F \subset \partial K$ means that F is a face of the d-dimensional rectangular subdomain. We can use the local estimators to form a global estimator of the error in the ith computed eigenfunction, given by

$$\eta^2_i = \sum_{K \in \mathcal{T}} \eta^2_{i,K}. \tag{3.11}$$

REMARK 3.2.   For hp-refinement, using the broken polynomial space, the constants γ_1 and γ_2 can be defined in terms of h_K and p_K [23, 19]; i.e.,

$$\gamma_1(p_K) = \frac{h^2_K}{p^2_K}, \quad \gamma_2(p_K) = \frac{h_K}{p_K}, \quad \alpha(p_K) = \frac{\gamma p^2_K}{h_K}. \tag{3.12}$$

Furthermore, it can be shown that

$$1 \lesssim \gamma p_K \le \gamma_2(p_K)\alpha(p_K), \tag{3.13}$$

i.e. the inequality (3.4) holds.

To quantify the error associated with the approximate solutions to the Kohn–Sham equations obtained from the DG approach, we need to define the following energy norm, which is induced from the bilinear form (2.21), and a corresponding distance function.

DEFINITION 3.3 (Energy norm). *For any $u \in H^1(\Omega) \oplus \mathcal{V}_{\mathcal{J}}(\mathcal{T})$,*

$$\|u\|_{E,\mathcal{T}}^2 := \sum_{K \in \mathcal{T}} \frac{1}{2} \|\nabla u_K\|^2 + \sum_{F \in \mathcal{S}} \alpha(J_F) \big\| [\![u]\!] \big\|_F^2. \tag{3.14}$$

DEFINITION 3.4. *For $v_{\mathcal{J}} \in \mathcal{V}_{\mathcal{J}}(\mathcal{T})$ and a finite dimensional subspace $\mathcal{P} \subset H_\pi^1(\Omega)$, the distance between $v_{\mathcal{J}}$ and $\mathcal{P}$ in the energy norm is defined as*

$$\mathrm{dist}(v_{\mathcal{J}}, \mathcal{P})_{E,\mathcal{T}} \equiv \inf_{w \in \mathcal{P}} \|v_{\mathcal{J}} - w\|_{E,\mathcal{T}}. \tag{3.15}$$

We now first give the main result for measuring the accuracy of the eigenfunctions using the a posteriori error estimator.

THEOREM 3.5 (Reliability of eigenfunctions). *Denote by $M(\varepsilon_i)$ the span of all eigenfunctions corresponding to the eigenvalue ε_i for the eigenvalue problem (2.13). Let $(\varepsilon_{i,\mathcal{J}}, u_{i,\mathcal{J}})$ be a computed eigenpair corresponding to (2.20) with $\varepsilon_{i,\mathcal{J}}$ converging to the true eigenvalue ε_i. If Assumption 3.1 holds, then*

$$\mathrm{dist}\,(u_{i,\mathcal{J}}, M(\varepsilon_i))_{E,\mathcal{T}} \lesssim \eta_i + (1 + \sqrt{\gamma_{1,\mathcal{J}}}) \inf_{\substack{u_i \in M(\varepsilon_i) \\ \|u_i\|_\Omega = 1}} \xi_i, \tag{3.16}$$

where

$$\xi_i^2 \equiv \sum_{K \in \mathcal{T}} \xi_{i,K}^2, \quad and \quad \xi_{i,K} = \|\varepsilon_i u_i - \varepsilon_{i,\mathcal{J}} u_{i,\mathcal{J}}\|_K + \|V_{\mathrm{eff}} u_i - V_{\mathrm{eff}} u_{i,\mathcal{J}}\|_K. \tag{3.17}$$

Proof. We decompose a computed eigenfunction $u_{i,\mathcal{J}}$ into a conforming part and a remainder part:

$$u_{i,\mathcal{J}} = u_{i,\mathcal{J}}^c + u_{i,\mathcal{J}}^r, \tag{3.18}$$

where $u_{i,\mathcal{J}}^c = I_{\mathcal{J}} u_{i,\mathcal{J}} \in H_\pi^1(\Omega)$ is defined using the interpolation operator satisfying the condition (3.5). From the triangle inequality,

$$\|u_i - u_{i,\mathcal{J}}\|_{E,\mathcal{T}} \le \big\|u_{i,\mathcal{J}}^r\big\|_{E,\mathcal{T}} + \big\|u_i - u_{i,\mathcal{J}}^c\big\|_{E,\mathcal{T}}, \tag{3.19}$$

it is sufficient to prove that both terms on the right hand side of Equation (3.19) are bounded by η_i. Applying lemmas A.1 and A.4 to Equation (3.19), we have

$$\|u_i - u_{i,\mathcal{J}}\|_{E,\mathcal{T}} \lesssim \eta_i + (1 + \sqrt{\gamma_{1,\mathcal{J}}})\xi_i. \tag{3.20}$$

The theorem follows from Equation (3.20) directly once we minimize ξ_i among all normalized eigenfunctions $u_i \in M(\varepsilon_i)$. □

Theorem 3.5 illustrates that the error of each eigenfunction attributed to the finite dimensional approximation $\mathcal{V}_{\mathcal{J}}$ is bounded by the residual-based error estimator η_i up to a constant factor independent of $\mathcal{V}_{\mathcal{J}}$ and a remaining term which is of higher order in the context of hp-refinement. As will be shown below, Theorem 3.5 is also used for error estimates of the eigenvalues. In the context of KSDFT, the error of eigenvalues directly indicates the error of physical observables such as total energies.

In order to develop a posteriori error estimates for eigenvalues, we need to address the technical difficulty that the bilinear operator $A_{\mathcal{J}}$ is neither coercive nor bounded with respect to the energy norm $\|\cdot\|_{E,\mathcal{T}}$ on the space $H_\pi^1(\Omega) \oplus \mathcal{V}_{\mathcal{J}}(\mathcal{T})$. We therefore need to extend the definition of the bilinear operator $A_{\mathcal{J}}$ in Equation (2.20). The extended bilinear operator is coercive and bounded on the joint space $H_\pi^1(\Omega) \oplus \mathcal{V}_{\mathcal{J}}(\mathcal{T})$, as will be shown in Lemma A.6. We introduce the lifting operator, which is used in [3, 23, 19] for hp-refinement, and generalize it to non-polynomial basis sets as follows.

DEFINITION 3.6 (Lifting operator). *For any $v \in H_\pi^1(\Omega) \oplus \mathcal{V}_{\mathcal{J}}(\mathcal{T})$, define $\mathcal{L}v \in \mathcal{W}_{\mathcal{J}}(\mathcal{T})$ by*

$$\langle \mathcal{L}v, \mathbf{q}_{\mathcal{J}} \rangle_{\mathcal{T}} \equiv \big\langle [\![v]\!], \{\!\{\mathbf{q}_{\mathcal{J}}\}\!\} \big\rangle_{\mathcal{S}}, \quad \forall \mathbf{q}_{\mathcal{J}} \in \mathcal{W}_{\mathcal{J}}(\mathcal{T}). \tag{3.21}$$

With the lifting operator, for any $u,v \in H_\pi^1(\Omega) \oplus \mathcal{V}_{\mathcal{J}}(\mathcal{T})$, we define the following extended bilinear form $\widetilde{A}_{\mathcal{J}}(u,v)$:

$$\widetilde{A}_{\mathcal{J}}(u,v) = \frac{1}{2}\langle \nabla u, \nabla v \rangle_{\mathcal{T}} - \frac{1}{2}\langle \mathcal{L}u, \nabla v \rangle_{\mathcal{T}} - \frac{1}{2}\langle \mathcal{L}v, \nabla u \rangle_{\mathcal{T}} + \sum_{F \in \mathcal{S}} \alpha(J_F)\big\langle [\![u]\!], [\![v]\!] \big\rangle_F. \tag{3.22}$$

It is clear that $\widetilde{A}_{\mathcal{J}}$ is consistent with both A and $A_{\mathcal{J}}$ in the sense that $\widetilde{A}_{\mathcal{J}}(u,v) = A(u,v)$, for all $u,v \in H_\pi^1(\Omega)$, and $\widetilde{A}_{\mathcal{J}}(u_{\mathcal{J}},v_{\mathcal{J}}) = A_{\mathcal{J}}(u_{\mathcal{J}},v_{\mathcal{J}})$, for all $u_{\mathcal{J}},v_{\mathcal{J}} \in \mathcal{V}_{\mathcal{J}}(\mathcal{T})$.

In the pseudopotential framework, V_{eff} is bounded from above and from below. Since any constant shift in the potential only causes the same constant shift in each Kohn–Sham eigenvalue ε_i without changing the Kohn–Sham orbitals, without loss of generality, we may add a positive constant to V_{eff}, if needed, so that V_{eff} is coercive and continuous on $H_\pi^1(\Omega) \oplus \mathcal{V}_{\mathcal{J}}(\mathcal{T})$; i.e.

$$\langle u,u \rangle_{\mathcal{T}} \lesssim \langle u, V_{\text{eff}}u \rangle_{\Omega} \lesssim \langle u,u \rangle_{\mathcal{T}}, \quad \forall u \in H_\pi^1(\Omega) \oplus \mathcal{V}_{\mathcal{J}}(\mathcal{T}). \tag{3.23}$$

This technique has also been used in previous work such as [18]. Combining Equation (3.23) with Lemma A.6, we have

$$\langle u,u \rangle_{\mathcal{T}} \lesssim \widetilde{A}_{\mathcal{J}}(u,u) + \langle V_{\text{eff}}u,u \rangle_{\mathcal{T}} \lesssim \langle u,u \rangle_{\mathcal{T}}. \tag{3.24}$$

Equation (3.24) implies that all true eigenvalues ε_i and computed eigenvalues $\varepsilon_{i,\mathcal{J}}$ are positive.

Using the extended bilinear form $\widetilde{A}_{\mathcal{J}}$, we can define the extended residual as follows.

DEFINITION 3.7 (Extended residual). *For any $v \in H_\pi^1(\Omega) \oplus \mathcal{V}_{\mathcal{J}}(\mathcal{T})$, and the eigenpair (ε_i, u_i), the extended residual corresponding to the eigenvalue problem (2.13) is*

$$\mathcal{R}(u_i,v) = \widetilde{A}_{\mathcal{J}}(u_i,v) + (u_i, V_{\text{eff}}v) - \varepsilon_i(u_i,v). \tag{3.25}$$

Similarly, for any $v \in H_\pi^1(\Omega) \oplus \mathcal{V}_{\mathcal{J}}(\mathcal{T})$ and the computed eigenpair $(\varepsilon_{i,\mathcal{J}}, u_{i,\mathcal{J}})$, the extended residual corresponding to the eigenvalue problem (2.20) is

$$\mathcal{R}_{\mathcal{J}}(u_{i,\mathcal{J}},v) = \widetilde{A}_{\mathcal{J}}(u_{i,\mathcal{J}},v) + (u_{i,\mathcal{J}}, V_{\text{eff}}v) - \varepsilon_{i,\mathcal{J}}(u_{i,\mathcal{J}},v). \tag{3.26}$$

Now we give the result used to measure the error of the eigenvalues using the a posteriori error estimator.

THEOREM 3.8 (Reliability of eigenvalues). *If Assumption 3.1 holds, let $(\varepsilon_{i,\mathcal{J}}, u_{i,\mathcal{J}})$ be a computed eigenpair corresponding to (2.20) with $\varepsilon_{i,\mathcal{J}}$ converging to the true eigenvalue ε_i of multiplicity greater than or equal to 1. Then we have*

$$|\varepsilon_i - \varepsilon_{i,\mathcal{J}}| \lesssim \eta_i^2 + \inf_{\substack{u_i \in M(\varepsilon_i) \\ \|u_i\|_\Omega = 1}} G_i, \tag{3.27}$$

where

$$G_i = (1 + \sqrt{\gamma_{1,\mathcal{J}}})^2 \xi_i^2 + 2\eta_i(1 + \sqrt{\gamma_{1,\mathcal{J}}})\xi_i + 2|\mathcal{R}(u_i, u_i - u_{i,\mathcal{J}})| + 2|\mathcal{R}_{\mathcal{J}}(u_{i,\mathcal{J}}, u_i - u_{i,\mathcal{J}})|. \tag{3.28}$$

Proof. Using Equation (A.45), $\|u_{i,\mathcal{J}}\|_{\mathcal{T}} = 1$, and $\varepsilon_i > 0$, we have

$$\begin{aligned}
\varepsilon_{i,\mathcal{J}} - \varepsilon_i &= \widetilde{A}_{\mathcal{J}}(u_i - u_{i,\mathcal{J}}, u_i - u_{i,\mathcal{J}}) + \langle V_{\mathrm{eff}}(u_i - u_{i,\mathcal{J}}), (u_i - u_{i,\mathcal{J}})\rangle_{\mathcal{T}} \\
&\quad - \varepsilon_i \|u_i - u_{i,\mathcal{J}}\|_\Omega^2 - 2\mathrm{Re}\mathcal{R}(u_i, u_i - u_{i,\mathcal{J}}) \\
&\leq \widetilde{A}_{\mathcal{J}}(u_i - u_{i,\mathcal{J}}, u_i - u_{i,\mathcal{J}}) + \langle V_{\mathrm{eff}}(u_i - u_{i,\mathcal{J}}), (u_i - u_{i,\mathcal{J}})\rangle_{\mathcal{T}} \\
&\quad + 2|\mathcal{R}(u_i, u_i - u_{i,\mathcal{J}})|.
\end{aligned} \tag{3.29}$$

Similarly, Equation (A.46) in Lemma A.8, $\|u_i\|_\Omega = 1$, and $\varepsilon_{i,\mathcal{J}} > 0$ give

$$\begin{aligned}
\varepsilon_i - \varepsilon_{i,\mathcal{J}} &= \widetilde{A}_{\mathcal{J}}(u_i - u_{i,\mathcal{J}}, u_i - u_{i,\mathcal{J}}) + \langle V_{\mathrm{eff}}(u_i - u_{i,\mathcal{J}}), (u_i - u_{i,\mathcal{J}})\rangle_{\mathcal{T}} \\
&\quad - \varepsilon_{i,\mathcal{J}} \|u_i - u_{i,\mathcal{J}}\|_\Omega^2 - 2\mathrm{Re}\mathcal{R}_{\mathcal{J}}(u_{i,\mathcal{J}}, u_{i,\mathcal{J}} - u_i) \\
&\leq \widetilde{A}_{\mathcal{J}}(u_i - u_{i,\mathcal{J}}, u_i - u_{i,\mathcal{J}}) + \langle V_{\mathrm{eff}}(u_i - u_{i,\mathcal{J}}), (u_i - u_{i,\mathcal{J}})\rangle_{\mathcal{T}} \\
&\quad + 2|\mathcal{R}_{\mathcal{J}}(u_{i,\mathcal{J}}, u_{i,\mathcal{J}} - u_i)|.
\end{aligned} \tag{3.30}$$

Combining equations (3.29) and (3.30), we have

$$\begin{aligned}
|\varepsilon_i - \varepsilon_{i,\mathcal{J}}| &\leq \widetilde{A}_{\mathcal{J}}(u_i - u_{i,\mathcal{J}}, u_i - u_{i,\mathcal{J}}) + \langle V_{\mathrm{eff}}(u_i - u_{i,\mathcal{J}}), u_i - u_{i,\mathcal{J}}\rangle_{\mathcal{T}} \\
&\quad + 2|\mathcal{R}(u_i, u_i - u_{i,\mathcal{J}})| + 2|\mathcal{R}_{\mathcal{J}}(u_{i,\mathcal{J}}, u_{i,\mathcal{J}} - u_i)|.
\end{aligned} \tag{3.31}$$

Using Equation (3.24), we obtain

$$|\varepsilon_i - \varepsilon_{i,\mathcal{J}}| \lesssim \|u_{i,\mathcal{J}} - u_i\|_{E,\mathcal{T}}^2 + 2|\mathcal{R}(u_i, u_i - u_{i,\mathcal{J}})| + 2|\mathcal{R}_{\mathcal{J}}(u_{i,\mathcal{J}}, u_i - u_{i,\mathcal{J}})| \tag{3.32}$$

which, using Equation (3.20) in Theorem 3.5, becomes

$$\begin{aligned}
|\varepsilon_i - \varepsilon_{i,\mathcal{J}}| &\lesssim \big(\eta_i + (1 + \sqrt{\gamma_{1,\mathcal{J}}})\xi_i\big)^2 + 2|\mathcal{R}(u_i, u_i - u_{i,\mathcal{J}})| + 2|\mathcal{R}_{\mathcal{J}}(u_{i,\mathcal{J}}, u_i - u_{i,\mathcal{J}})| \\
&\equiv \eta_i^2 + G_i.
\end{aligned} \tag{3.33}$$

The theorem then follows directly from Equation (3.33) once we minimize G_i among all normalized eigenfunctions $u_i \in M(\varepsilon_i)$. $\square$

REMARK 3.9. It remains to be shown that η_i dominates ξ_i in Equation (3.16). To this end, we require a priori estimates of the convergence rate of $u_{i,\mathcal{J}}$, which we do not have at this stage. However, in the case of standard hp-refinement for the Laplacian eigenvalue

problem, it can be shown that ξ_i is of a higher order than $\mathrm{dist}\,(u_{i,\mathcal{J}}, M(\varepsilon_i))_{E,\mathcal{T}}$ [19]. This implies that η_i is the leading order term in the estimate of the eigenfunctions (3.16).

Similarly, in the case of standard hp-refinement for solving the Laplacian eigenvalue problem, it can be shown that $\mathcal{R}(u_i, u_i - u_{i,\mathcal{J}})$ is of a higher order than $|\varepsilon_i - \varepsilon_{i,\mathcal{J}}|$. One can also show that $\mathcal{R}_{\mathcal{J}}(u_{i,\mathcal{J}}, u_i - u_{i,\mathcal{J}})$ is of a higher order than $|\varepsilon_i - \varepsilon_{i,\mathcal{J}}|$. Combining this with the statement above, we can then conclude that η_i^2 is the leading order term in the estimate of the eigenvalues (3.27) in this case.

For general basis sets, the proof that these terms are of higher order relies on an *a priori* error analysis of the basis set. According to our current understanding, this analysis might be even more difficult than the *a posteriori* error analysis given here for general non-polynomial basis functions.

3.2. Non-uniform adaptive local basis refinement strategy.   Theorem 3.5 demonstrates that the a posteriori error estimator is reliable in quantifying the error of each eigenfunction on the global domain for a suitable set of local basis functions. In practical calculations, we use the local error estimator $\eta_{i,K}$ to guide the adaptive refinement of the basis functions. An accurate and efficient solution should not be under-resolved nor over-resolved in any element; thus a non-uniform local basis refinement strategy should yield a solution for which the value of the local estimator is close to uniform across all elements.

Since we are concerned with the error of all eigenpairs simultaneously, we define the local estimator on an element K by

$$\eta_K^2 = \sum_{i=1}^{N} \eta_{i,K}^2. \tag{3.34}$$

The refinement strategy is straightforward. Minimum and maximum local error thresholds, ϵ_{min} and ϵ_{max}, are chosen based on the desired global error, along with a basis refinement step size b_{step} and a number of refinement steps n. An initial distribution of basis functions $\mathcal{J}_1$, which may be uniform or, given prior knowledge of the problem, non-uniform, is also specified. A trial solution is computed using the initial distribution $\mathcal{J}_1$. The local estimators η_K^2 are evaluated. For each element K, if $\eta_K^2 < \epsilon_{min}$, b_{step} local basis functions are removed from K. If $\eta_K^2 > \epsilon_{max}$, b_{step} local basis functions are added to K. Thus, local basis functions are removed from over-resolved elements and added to under-resolved elements. At each iteration j, Equation (2.27) is solved for the lowest $J_{K,j}$ eigenfunctions to obtain the adaptive local basis functions. A new solution is computed, and the process is repeated. On the $(n-1)$st step, a final distribution of basis functions $\mathcal{J}_n$ is determined, and the electron density ρ is computed using this distribution. This procedure is outlined in Algorithm 1.

This strategy may not yield an efficient distribution of basis functions if the initial distribution $\mathcal{J}_1$ contains too few basis functions to reasonably resolve the system, nor is it intended to do so. In this case, the local estimator may not be effective at the first step which could lead to erratic estimates of local error. It is not necessarily the case that the total number of basis functions will increase as the basis is refined—as we will demonstrate in Section 4, the total number of basis functions may very well decrease through the refinement process—so all available resources may be used to make the initial calculation. Rather, the refinement process redistributes basis functions to achieve higher accuracy at a minimum cost by adding basis functions to under-resolved elements and removing basis functions from over-resolved elements.

Let us contrast the non-uniform refinement procedure with a uniform refinement procedure in which some number b_{step} of basis functions are added to every element

---

Algorithm 1 Non-uniform basis refinement procedure.

Input: $\epsilon_{\min}$, $\epsilon_{\max}$, initial distribution of basis functions $\mathcal{J}_1 = \{J_{K,1}\}_{K \in \mathcal{T}}$, n, b_{step}

Output: Refined distribution of basis functions $\mathcal{J}_n$ and physical quantities such as electron density ρ

for $1 \leq j \leq n-1$ **do**

    Compute a set of eigenpairs $\{(\varepsilon_{i,\mathcal{J}_j}, u_{i,\mathcal{J}_j})\}_{i=1}^N$ based on the ALB approach

    for $K \in \mathcal{T}$ **do**

        Compute η_K^2

        if $\eta_K^2 < \epsilon_{\min}$ **then**

            Update $J_{K,j+1} \leftarrow \max(J_{K,j} - b_{\text{step}}, 0)$

        else if $\eta_K^2 > \epsilon_{\max}$ **then**

            Update $J_{K,j+1} \leftarrow J_{K,j} + b_{\text{step}}$

        else

            Update $J_{K,j+1} \leftarrow J_{K,j}$

        end if

    end for

end for

Compute and output physical quantities (such as ρ) using $\mathcal{J}_n$

---

for each of the n steps. If we carry out uniform and non-uniform refinement with the same choices of b_{step} and n and the same initial distribution of basis functions $\mathcal{J}_1$, we can compare the accuracy and total number of basis functions used at each step of the two refinement processes. The maximum possible number of basis functions assigned to any element on a given step of the non-uniform refinement scheme will always be equal to the number of basis functions in all elements on the same step of the uniform refinement scheme, but the minimum number of basis functions assigned to any element may be as little as zero. Therefore, the error on a given step of the uniform refinement scheme will always be less than or equal to that on the corresponding step of the non-uniform refinement scheme, up to small numerical errors incurred during the course of the solution process. We may then ask how much less is the error obtained from uniform refinement than from non-uniform refinement and how many more basis functions are used to make it so. This is the criterion by which the non-uniform refinement scheme will be judged against a uniform refinement scheme for the calculations presented in Section 4.

4. Numerical results for Kohn–Sham density functional theory calculations

In this section, we present numerical results which demonstrate that the global estimator is effective in predicting the error of the total energy, and that the local estimator may be used to guide efficient non-uniform local basis refinement. Although the theoretical part of the paper only aims at developing an a posteriori error estimator for linear eigenvalue problems, we apply the estimator to solve the nonlinear Kohn–Sham equations. All numerical results are performed with converged self-consistent field iterations. They properly take into account the nonlinearity of the Kohn–Sham equations. We test the refinement strategy for Kohn–Sham density functional theory calculations on two example systems. The first is an aluminum surface with a large vacuum region, and the second is a single layer of graphene oxide in water. These systems are highly inhomogeneous and therefore serve as good benchmark examples of non-uniform adaptive local basis refinement.

The evaluation of the a posteriori error estimator and the refinement strategy are implemented in the Discontinuous Galerkin Density Functional Theory (DGDFT) software. The energies and atomic forces are directly compared with the results obtained from ABINIT [20] using the same atomic configuration. We note that although the analysis in Section 3 is given for the linear eigenvalue problem, in all the numerical examples we solve the nonlinear eigenvalue problem as is required for KSDFT calculations. The results presented for both DGDFT and for ABINIT calculations have achieved convergence in the self-consistent field (SCF) iteration. In both the DGDFT and the ABINIT calculations, we use the local density approximation (LDA) [8, 34] for the exchange-correlation functional and the Hartwigsen–Goedecker–Hutter (HGH) pseudopotential [21] with the local and non-local pseudopotential fully implemented in the real space [32]. All quantities are reported in atomic units (au). All calculations are carried out on the Edison system maintained at the National Energy Research Scientific Computing Center (NERSC). Each compute node on Edison has 24 Intel "Ivy Bridge" cores (2.4 GHz) with 64 gigabytes (GB) of memory.

As a first attempt, we use the choice of parameters in Equation (3.12) to define the a posteriori error estimator. We define h_K to be the diameter of the element K, and we reinterpret p_K to be the number of ALBs rather than the polynomial degree in each element K. Our results indicate that, for the examples studied, the global estimator $\eta^2 = \sum_{K \in \mathcal{T}} \eta_K^2$ is numerically effective in predicting the error of the total energy within a relatively small constant factor, and that the local estimator η_K^2 is numerically effective in predicting the error in each element K of the computed electron density ρ. As a result, the non-uniform basis refinement strategy yields efficient distributions of local basis functions across the elements for these examples. Replacing a uniform refinement scheme with a non-uniform refinement scheme incurs very little loss in accuracy but allows the use of a much smaller basis and hence gives significant computational savings.

4.1. Quasi-2D aluminum surface. The first example is a quasi-2D aluminum surface with a large vacuum region. The periodic domain contains 16 aluminum atoms arranged in a row and a large vacuum region. The size of the supercell is approximately 7.65 au, 30.61 au, and 45.92 au along the x, y, and z directions, respectively. The computational domain is partitioned into a $1 \times 6 \times 9$ grid of elements. The size of the extended element is always 3 times the size of the element along each direction, unless there is only one element, and in this case, the size of the extended element is the same as the size of the element. One slice of the electron density ρ in the y-z plane is shown in Figure 4.1a and another in the x-y plane in Figure 4.1b. The black dashed lines indicate the partition of the elements. In DGDFT, a uniform grid is used to represent quantities such as the electron density and potential in the global domain with 70, 276, and 414 grid points along the x, y, and z directions, respectively. A Legendre–Gauss–Lobatto (LGL) grid is used inside each element to construct the DG Hamiltonian matrix, and the number of LGL grid points inside each element is 140, 92, and 92 along the x, y, and z directions, respectively.

Figure 4.2 shows the pointwise error of the electron density corresponding to the slice shown in Figure 4.1a with 50 adaptive local basis functions used in each element. The error of the density ρ is highly non-uniform across different elements; the error in the elements which contain atoms can be more than 5 orders of magnitude larger than that in elements in the vacuum region.

Figure 4.3a shows the slice of electron density along $y = 7.6534$ as indicated by the green dash-dotted line in Figure 4.1a. Figure 4.3b shows the error of the electron density along with the values of the local estimator η_K^2 in each of the elements K through which
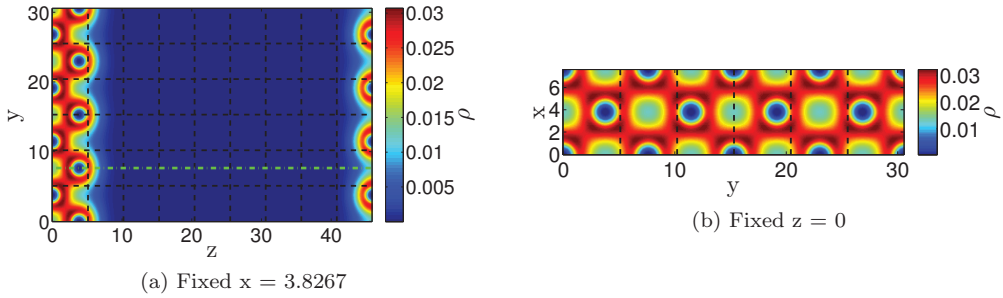
(a) Fixed x = 3.8267

(b) Fixed z = 0

Fig. 4.1: *Electron density ρ in the (a) y-z plane and in the (b) x-y plane. The partition of the global domain into 1×6×9 elements is indicated by black dashed lines.*
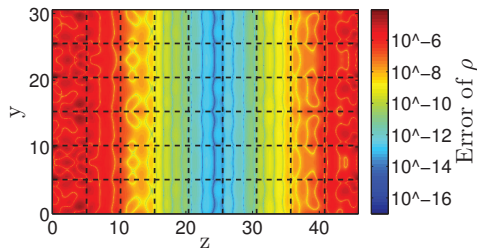

Fig. 4.2: *The pointwise error of the electron density ρ (in log scale) for the slice shown in Figure 4.1a when 50 adaptive local basis functions are used in each element. The error varies in different elements by several orders of magnitude which indicates that non-uniform distribution of basis functions may be used to generate more efficient electronic structure calculations for this system. The error is computed by comparing with the DGDFT result an accurate calculation obtained using the software package ABINIT.*

(a) Electron density

(b) Pointwise error of slice and local estimator
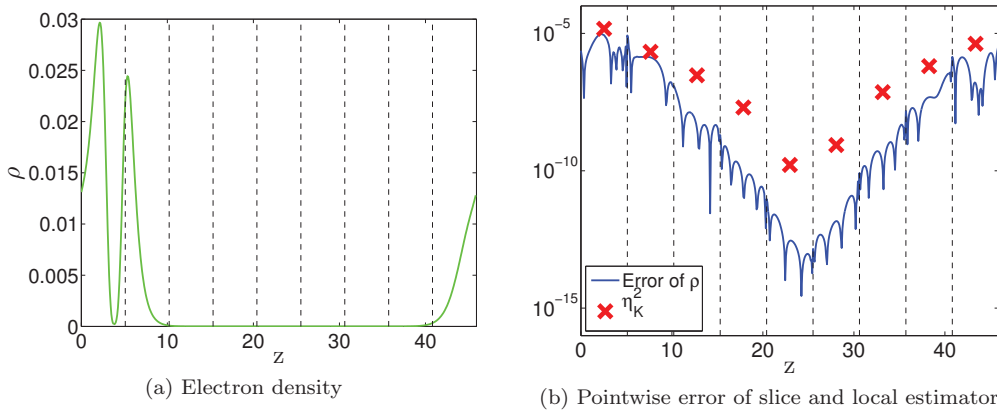
Fig. 4.3: *(a) One-dimensional slice of the electron density indicated by the green dash-dotted line in Figure 4.1a at y = 7.6534. (b) The error of the electron density along with the local estimator η_K^2 along the one dimensional slice demonstrating the effectiveness of the local estimator at predicting the local error of ρ.*
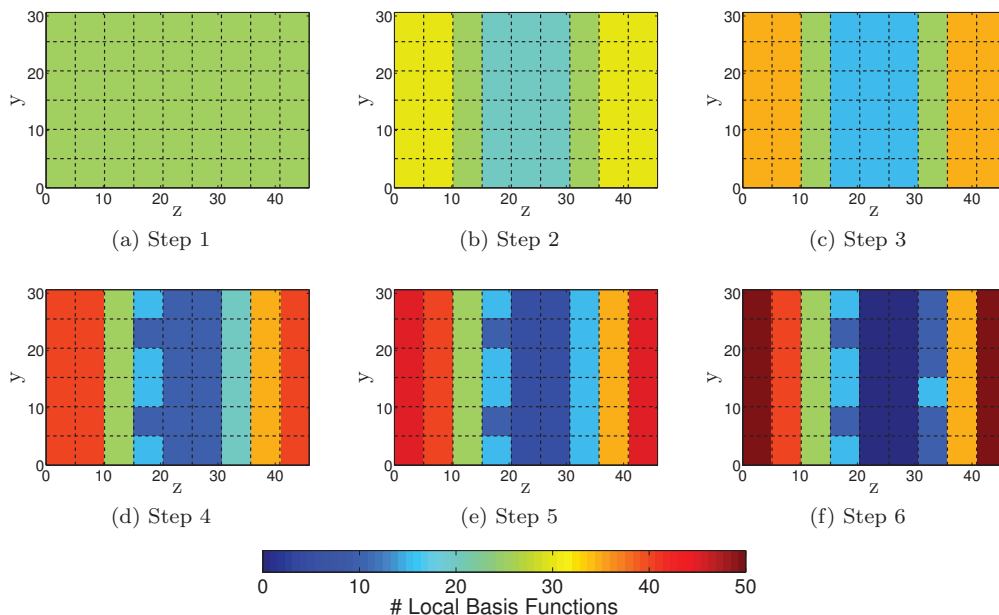
Fig. 4.4: *Distribution of adaptive local basis functions in six steps of non-uniform refinement for aluminum system. The final distribution mirrors the pointwise errors shown in Figure 4.2.*

the slice passes. We observe that the local estimator provides an upper bound for the local error of the electron density and can be used to indicate the relative contributions of the various elements to this error in the adaptive refinement procedure.

Let us next compare the accuracy and efficiency of uniform and non-uniform basis refinement schemes for this system. In both schemes, we begin with 25 adaptive local basis functions in all elements on the first step. We specify the basis refinement step size $b_{\mathrm{step}} = 5$ and the number of steps $n = 6$. In the uniform refinement scheme, we simply add $b_{\mathrm{step}} = 5$ basis functions to each element on each step. The non-uniform refinement scheme follows Algorithm 1 with $\epsilon_{\max} = 5 \times 10^{-6}$ and $\epsilon_{\min} = 5 \times 10^{-7}$.

We first examine the distribution of basis functions produced by the non-uniform refinement scheme, shown for all steps in Figure 4.4. The scheme eventually places more basis functions in elements for which a uniform distribution of basis functions produces larger pointwise errors. This becomes clear when comparing figures 4.4 and 4.2, the latter of which gives the pointwise error in the density for the last step of the uniform refinement scheme. Indeed, the non-uniform scheme allocates *zero basis functions* to the elements which contain the smallest pointwise errors in the uniform scheme and the maximum possible number of basis functions to the elements which contain the largest pointwise errors in the uniform scheme.

At the last step of refinement, the non-uniform refinement scheme uses half as many basis functions per atom as the uniform refinement scheme, as shown in Figure 4.5c. These savings are obtained without sacrificing accuracy. Figure 4.5a show that the error per atom of the total energy is nearly equal using both methods, despite the large difference in the number of basis functions used. We also measure the accuracy of the atomic force which is given by the derivative of the energy with respect to the atomic positions. The atomic force is used in various applications including geometry
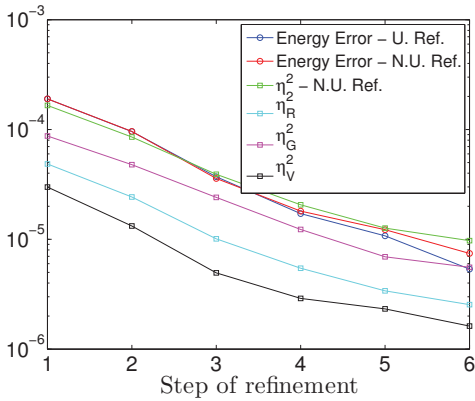
(a) Error per atom of total energy (Hartree/atom) for uniform refinement (U. Ref.) and non-uniform refinement (N.U. Ref) along with the global estimator. We also show the individual terms of the estimator summed over all elements $K \in \mathcal{T}$: the residual η_R^2, the discontinuity of the gradient η_G^2, and the discontinuity of the function values η_V^2.
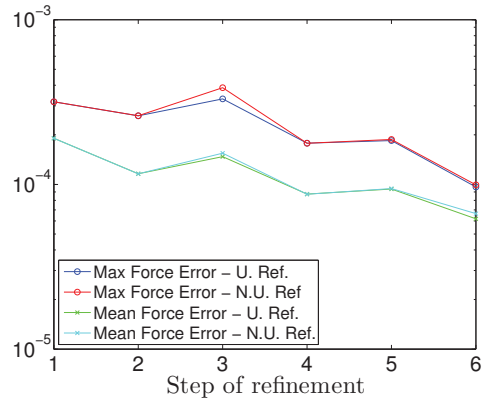
(b) Error of atomic force (au) for uniform and non-uniform refinement.
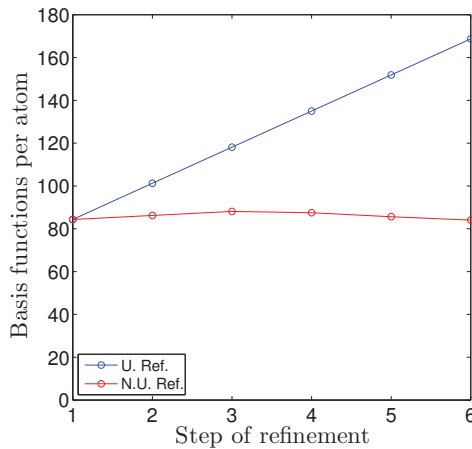
(c) Number of basis functions per atom for uniform and non-uniform refinement.

Fig. 4.5: *Accuracy and savings for aluminum system calculations. The non-uniform refinement scheme produces results which are nearly as accurate as those produced by the uniform refinement scheme using only half as many basis functions.*

optimization and molecular dynamics. We measure both the maximum and the average Euclidean error of the atomic forces among all atoms. Figure 4.5b shows that both accuracy measurements are nearly the same using uniform and non-uniform refinement. We therefore see that non-uniform refinement significantly improves the efficiency of the adaptive local basis functions by simply redistributing basis functions according to the predictions of the local estimator without sacrificing accuracy.

We lastly demonstrate that the use of non-uniformly distributed adaptive local basis functions gives significant savings over the use of planewave basis functions as in
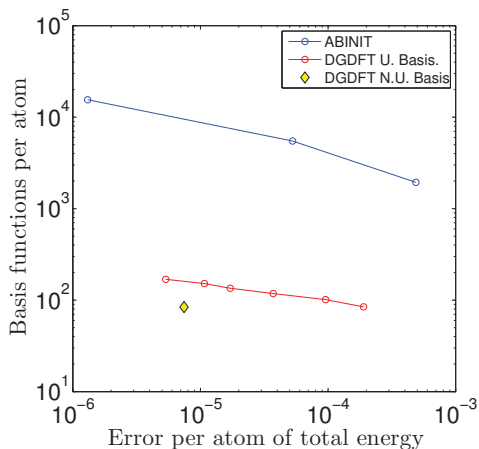
Fig. 4.6: *Number of basis functions used to achieve a given error of the total energy for the aluminum example. Non-uniform adaptive local basis sets obtained from DGDFT are approximately two orders of magnitude smaller than planewave basis sets obtained from ABINIT for similar error.*
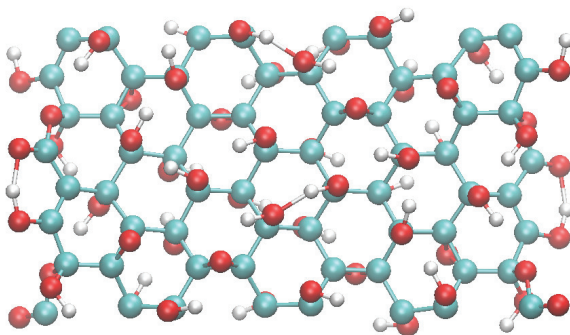

Fig. 4.7: *Atomic configuration of a single layer of graphene oxide in water with* 160 *atoms.*

ABINIT. The number of basis functions in planewave-based electronic structure calculations is usually denoted by the kinetic energy cutoff (E_{cut}). In atomic units, the relation between the total number N_{pw} of basis functions used in a planewave calculation and E_{cut} is approximately (depending on adjustments to the number of grid points for performance improvements) [30]

$$N_{\mathrm{pw}} = \left(\frac{\sqrt{2E_{\mathrm{cut}}}}{\pi} \right)^3 \mathrm{Vol}, \tag{4.1}$$

where Vol is the volume of the computational domain.

Figure 4.6 plots the number of basis functions per atom against the error per atom of the total energy using the planewave basis set obtained from ABINIT, a uniform distribution of adaptive local basis functions obtained from DGDFT, and a non-uniform distribution of adaptive local basis functions obtained from DGDFT. We observe that DGDFT calculations use many fewer basis functions than ABINIT calculations to achieve similar error. For example, to achieve an error of the total energy on the order
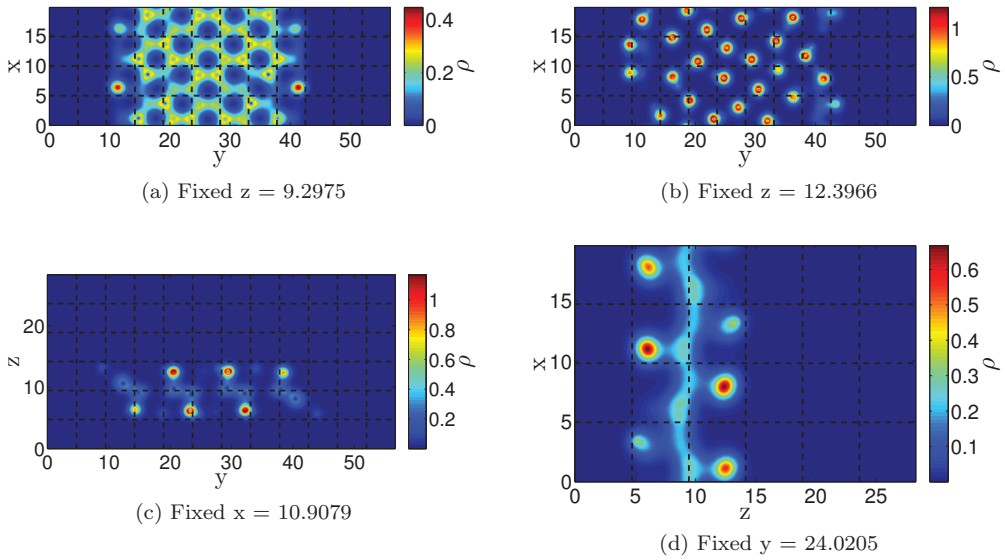
(a) Fixed z = 9.2975

(b) Fixed z = 12.3966

(c) Fixed x = 10.9079

(d) Fixed y = 24.0205

Fig. 4.8: *Two-dimensional slices of electron density for the graphene oxide system with a 4 × 12 × 6 grid used in DGDFT calculations indicated by black dashed lines.*

(a) Fixed z = 9.2975

(b) Fixed z = 12.3966

(c) Fixed x = 10.9079
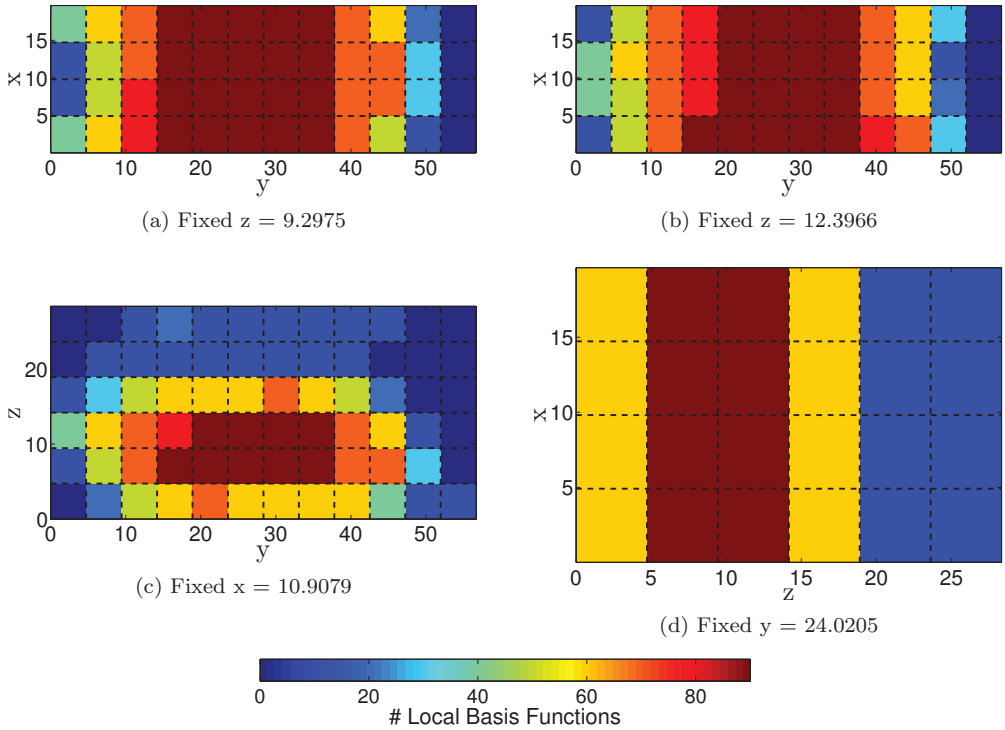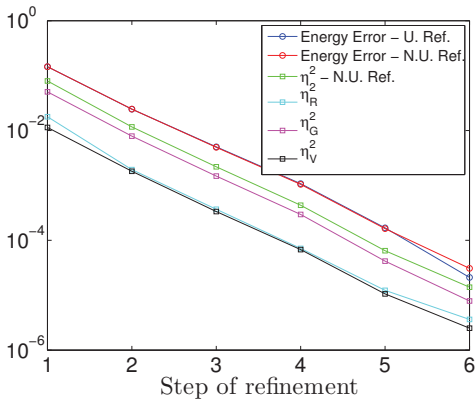
(d) Fixed y = 24.0205

Local Basis Functions

Fig. 4.9: *Distributions of adaptive local basis functions at the last step of non-uniform refinement in the elements containing the slices shown in Figure 4.8. The distribution of basis functions closely reflects the density.*

(a) Error per atom of total energy (Hartree/atom) for uniform refinement (U. Ref.) and non-uniform refinement (N.U. Ref) along with the global estimator. We also show the individual terms of the estimator summed over all elements $K \in \mathcal{T}$: the residual η_R^2, the discontinuity of the gradient η_G^2, and the discontinuity of the function values η_V^2.
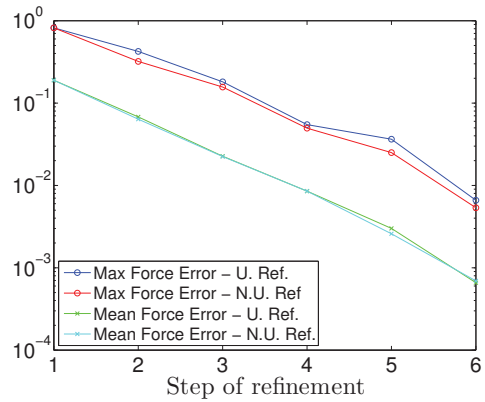
(b) Error of atomic force (au) for uniform and non-uniform refinement.
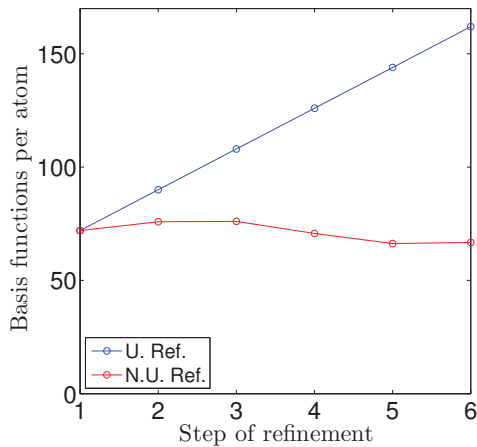
(c) Number of basis functions per atom for uniform and non-uniform refinement.

Fig. 4.10: *Accuracy and savings for graphene oxide system calculations. As in the aluminum case, the non-uniform refinement scheme is nearly as accurate and more efficient than the uniform scheme, and the global estimator is asymptotically effective.*

of 10^{-6} Hartree per atom, ABINIT requires around 10,000 planewave basis functions per atom, whereas DGDFT requires approximately 84 adaptive local basis functions per atom when non-uniform basis refinement is used.

4.2. Graphene oxide.   We next consider a layer of graphene oxide in water consisting of 160 atoms with the atomic configuration shown in Figure 4.7. The size of the supercell is 19.63 au, 56.69 au, and 28.35 au along the x, y, and z directions, respectively. The computational domain is partitioned into a $4 \times 12 \times 6$ grid of elements. As in the case of the aluminum system, a uniform grid is used to represent quantities
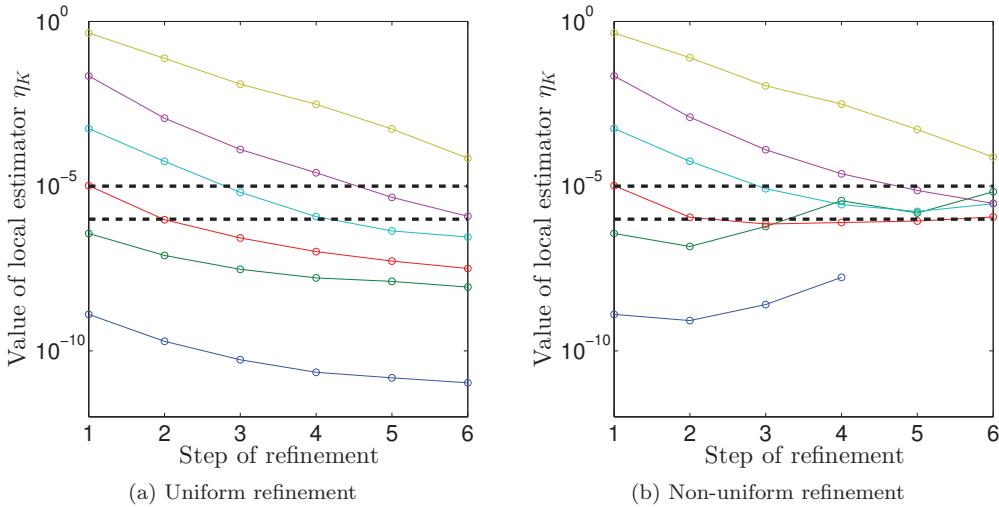
Fig. 4.11: *Quintile values of the local estimator for uniform and non-uniform basis refinement along with $\epsilon_{\max}$ and $\epsilon_{\min}$. The dominant local errors are roughly the same in both elements, but the non-uniform refinement scheme produces savings in the elements with small local error. Note that the minimum value of the local estimator across all elements becomes 0 by the fifth step of non-uniform refinement.*

such as the electron density and potential in the global domain in DGDFT, with 160, 456, and 228 grid points along the x, y, and z directions, respectively. A Legendre–Gauss–Lobatto (LGL) grid is used inside each element to construct the DG Hamiltonian matrix, and the number of LGL grid points inside each element is 80, 76, and 76 along the x, y, and z directions, respectively. Figure 4.8 shows slices of the density across various planes.

We perform both uniform and non-uniform refinement of the basis functions. We begin with a uniform distribution of 40 basis functions in each element for both schemes. The basis refinement step size is set at $b_{\text{step}} = 10$ and the number of refinement steps is set at $n = 6$. For the non-uniform refinement scheme, we use $\epsilon_{max} = 10^{-4}$ and $\epsilon_{min} = 10^{-6}$. Figure 4.9 shows the final distributions of adaptive local basis functions generated by the non-uniform refinement process in the elements containing the slices shown in Figure 4.8. The distribution of adaptive local basis functions corresponds well to the highly inhomogeneous electron density of the system.

Figure 4.10 demonstrates the accuracy and efficiency of the non-uniform refinement procedure for the graphene oxide calculation. Figure 4.10a shows that the difference in the error of the total energy per atom for the two refinement schemes is very small and that the global estimator is highly effective in capturing the error of the total energy. The maximum and average errors of the atomic forces among all the atoms are given in Figure 4.10b for the uniform and non-uniform refinement schemes, which again give similar accuracy. Figure 4.10c shows that by the final step of refinement the uniform refinement scheme uses nearly 2.5 times as many basis functions as the non-uniform refinement scheme. Furthermore, the non-uniform refinement scheme uses fewer basis functions at the final step than it does at the first step, though the error is four orders of magnitude lower.

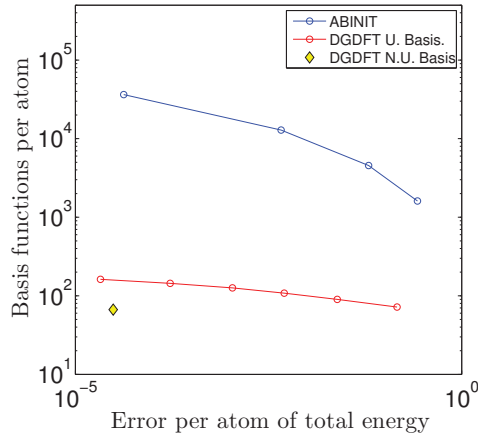Another perspective on the effectiveness of the non-uniform refinement strategy is

Fig. 4.12: *Number of basis functions used to achieve a given error of the total energy for the GO example. Non-uniform adaptive local basis sets obtained from DGDFT are approximately three orders of magnitude smaller than planewave basis sets obtained from ABINIT for similar error.*

given in Figure 4.11 in which we plot the quintile values of the local estimator across all elements at each step of uniform and non-uniform refinement along with the error thresholds $\epsilon_{\max}$ and $\epsilon_{\min}$. In the uniform refinement scheme, both under- and over-resolved elements become further refined at each step. In the non-uniform refinement scheme, only the under-resolved elements are further refined; the over-resolved elements are instead made less refined at each step, thus recovering inefficiently-allocated resources. The dominant sources of error are similar in both cases, so very little loss in accuracy is incurred by using a non-uniform basis refinement scheme.

Figure 4.12 compares the number of planewave basis functions used by ABINIT with the number of adaptive local basis functions used by DGDFT to achieve similar error for the graphene oxide example. We observe, for example, that to achieve an error of the total energy on the order of 10^{-5} Hartree per atom, ABINIT requires around 35,000 planewave basis functions per atom, whereas DGDFT requires approximately 67 adaptive local basis functions per atom when non-uniform basis refinement is used.

5. Conclusion and future work

In this paper, we develop residual-based a posteriori local error estimates for solving KSDFT using adaptive local basis functions in a discontinuous Galerkin framework. Compared with standard hp-refinement, the major difficulty in carrying out the analysis is that little is known about the analytical properties of the adaptive local basis functions. We therefore effectively need to perform an a posteriori error analysis for general non-polynomial basis functions. In order to proceed, we postulate a set of assumptions on the basis set under which we are able to prove that the a posteriori error estimator is an upper bound for the errors of both eigenvalues and eigenvectors up to terms which are of higher order in the context of standard hp-refinement. We acknowledge that there is still difficulty in verifying the assumptions for a specific non-polynomial basis set such as the ALBs. We plan to carry out a numerical verification of the assumptions for the adaptive local basis functions in the future. The hope is that such a study can illuminate the approximation properties of the ALB sets from an analytic point of view

and also inform the a priori error analysis.

From a practical point of view, the results given by the local error estimator used in DGDFT mimic the *hp*-refinement results. As a first attempt, we reinterpret *p* as the number of adaptive local basis functions used in each element. We consider this only as a starting point for the study, but nevertheless, the numerical results show that the approach of a posteriori error estimates is promising for KSDFT studies. We demonstrate the practical use of the a posteriori error estimator for three-dimensional KSDFT calculations for quasi-2D aluminum surfaces and a single layer graphene oxide system in water. Besides the systems with a vacuum region, we also plan to use the non-uniform refinement strategy to study systems with defects and dislocations. In these cases, the electron density and the magnitude of the estimator may not vary as much as in the case of a large vacuum region.

Besides the adaptive refinement, another important application of a posteriori error estimation is to capture the error due to the finite dimensional approximation of physical quantities, such as total energies, without performing a more refined calculation which can be prohibitively expensive in practical KSDFT calculations. The error of the total energy is directly related to the error of eigenvalues. However, this objective requires a much more precise estimator than is used in the current formulation, and this will be our future work.

Appendix A. Details for proving Theorem 3.5 and 3.8.

LEMMA A.1. *Let $u_{i,\mathcal{J}}^r$ be defined as in Equation* (3.18), *then*

$$\left\| u_{i,\mathcal{J}}^r \right\|_{E,\mathcal{T}} \lesssim \eta_i. \tag{A.1}$$

Proof. Using Equation (3.5),

$$\sum_{K\in\mathcal{T}} \left\| \nabla u_{i,\mathcal{J}}^r \right\|_K^2 \lesssim \sum_{F\in\mathcal{S}} \gamma_2(J_F)\alpha^2(J_F) \left\| [\![u_{i,\mathcal{J}}]\!] \right\|_F^2 \lesssim \sum_{K\in\mathcal{T}} \eta_{i,V_K}^2 \leq \eta_i^2. \tag{A.2}$$

Using Equation (3.4),

$$\sum_{F\in\mathcal{S}} \alpha(J_F) \left\| [\![u_{i,\mathcal{J}}]\!] \right\|_F^2 \lesssim \sum_{F\in\mathcal{S}} \gamma_2(J_F)\alpha^2(J_F) \left\| [\![u_{i,\mathcal{J}}]\!] \right\|_F^2 \lesssim \sum_{K\in\mathcal{T}} \eta_{i,V_K}^2 \leq \eta_i^2. \tag{A.3}$$

Then Lemma A.1 follows directly from the definition of the energy norm (3.14). ☐

DEFINITION A.2 (Split of $A_\mathcal{J}$). *The bilinear form $A_\mathcal{J}$ in Equation* (2.21) *can be split into two parts:*

$$A_\mathcal{J}(u,v) = D_\mathcal{J}(u,v) + K_\mathcal{J}(u,v). \tag{A.4}$$

Here

$$D_{\mathcal{J}}(u,v) = \frac{1}{2}\langle \nabla u, \nabla v\rangle_{\mathcal{T}} + \sum_{F\in\mathcal{S}}\alpha(J_F)\langle [\![u]\!], [\![v]\!]\rangle_F, \tag{A.5}$$

and

$$K_{\mathcal{J}}(u,v) = -\frac{1}{2}\langle \{\!\{\nabla u\}\!\}, [\![v]\!]\rangle_{\mathcal{S}} - \frac{1}{2}\langle \{\!\{\nabla v\}\!\}, [\![u]\!]\rangle_{\mathcal{S}}. \tag{A.6}$$

Formally, it is clear that

$$A(u,v) = D_{\mathcal{J}}(u,v), \quad \forall u,v\in H^1_\pi(\Omega). \tag{A.7}$$

LEMMA A.3. *If Assumption 3.1 holds, let $(\varepsilon_{i,\mathcal{J}}, u_{i,\mathcal{J}})$ be a computed eigenpair corresponding to (2.20), and let (ε_i, u_i) an eigenpair corresponding to (2.25). For any $v\in H^1_\pi(\Omega)$, let $v_{\mathcal{J}}\in\mathcal{V}_{\mathcal{J}}(\mathcal{T})$ satisfy (3.1) and (3.2). Then we have*

$$\langle \varepsilon_i u_i - V_{\text{eff}} u_i, v - v_{\mathcal{J}}\rangle_{\mathcal{T}} - D_{\mathcal{J}}(u_{i,\mathcal{J}}, v - v_{\mathcal{J}}) + K_{\mathcal{J}}(u_{i,\mathcal{J}}, v_{\mathcal{J}}) \lesssim \left(\eta_i + \sqrt{\gamma_{1,\mathcal{J}}}\xi_i\right)\|v\|_{E,\mathcal{T}}. \tag{A.8}$$

Proof. For brevity, set

$$T = \langle \varepsilon_i u_i - V_{\text{eff}} u_i, v - v_{\mathcal{J}}\rangle_{\mathcal{T}} - D_{\mathcal{J}}(u_{i,\mathcal{J}}, v - v_{\mathcal{J}}) + K_{\mathcal{J}}(u_{i,\mathcal{J}}, v_{\mathcal{J}}). \tag{A.9}$$

Integrating by parts gives

$$D_{\mathcal{J}}(u_{i,\mathcal{J}}, v - v_{\mathcal{J}}) = -\sum_{K\in\mathcal{T}}\frac{1}{2}\langle \Delta u_{i,\mathcal{J}}, v - v_{\mathcal{J}}\rangle_K + \sum_{F\in\mathcal{S}}\alpha(J_F)\langle [\![u_{i,\mathcal{J}}]\!], [\![v - v_{\mathcal{J}}]\!]\rangle_F$$
$$+ \sum_{K\in\mathcal{T}}\frac{1}{2}\langle \nabla u_{i,\mathcal{J}}\cdot\mathbf{n}_K, v - v_{\mathcal{J}}\rangle_{\partial K}. \tag{A.10}$$

Using the identity

$$\sum_{K\in\mathcal{T}}\langle \nabla u_{i,\mathcal{J}}\cdot\mathbf{n}_K, v - v_{\mathcal{J}}\rangle_{\partial K} = \sum_{F\in\mathcal{S}}\langle \{\!\{\nabla u_{i,\mathcal{J}}\}\!\}, [\![v - v_{\mathcal{J}}]\!]\rangle_F$$
$$+ \sum_{F\in\mathcal{S}}\langle [\![\nabla u_{i,\mathcal{J}}]\!], \{\!\{v - v_{\mathcal{J}}\}\!\}\rangle_F, \tag{A.11}$$

we have

$$T = \sum_{K\in\mathcal{T}}\left\langle \varepsilon_i u_i + \frac{1}{2}\Delta u_{i,\mathcal{J}} - V_{\text{eff}} u_i, v - v_{\mathcal{J}}\right\rangle_K - \sum_{F\in\mathcal{S}}\alpha(J_F)\langle [\![u_{i,\mathcal{J}}]\!], [\![v - v_{\mathcal{J}}]\!]\rangle_F$$
$$- \sum_{F\in\mathcal{S}}\frac{1}{2}\langle \{\!\{\nabla u_{i,\mathcal{J}}\}\!\}, [\![v - v_{\mathcal{J}}]\!]\rangle_F - \sum_{F\in\mathcal{S}}\frac{1}{2}\langle [\![\nabla u_{i,\mathcal{J}}]\!], \{\!\{v - v_{\mathcal{J}}\}\!\}\rangle_F$$
$$- \sum_{F\in\mathcal{S}}\frac{1}{2}\langle \{\!\{\nabla u_{i,\mathcal{J}}\}\!\}, [\![v_{\mathcal{J}}]\!]\rangle_F - \sum_{F\in\mathcal{S}}\frac{1}{2}\langle \{\!\{\nabla v_{\mathcal{J}}\}\!\}, [\![u_{i,\mathcal{J}}]\!]\rangle_F$$
$$= \sum_{K\in\mathcal{T}}\left\langle \varepsilon_i u_i + \frac{1}{2}\Delta u_{i,\mathcal{J}} - V_{\text{eff}} u_i, v - v_{\mathcal{J}}\right\rangle_K - \sum_{F\in\mathcal{S}}\alpha(J_F)\langle [\![u_{i,\mathcal{J}}]\!], [\![v - v_{\mathcal{J}}]\!]\rangle_F$$
$$- \sum_{F\in\mathcal{S}}\frac{1}{2}\langle [\![\nabla u_{i,\mathcal{J}}]\!], \{\!\{v - v_{\mathcal{J}}\}\!\}\rangle_F - \sum_{F\in\mathcal{S}}\frac{1}{2}\langle \{\!\{\nabla v_{\mathcal{J}}\}\!\}, [\![u_{i,\mathcal{J}}]\!]\rangle_F$$

$$\equiv T_1 + T_2 + T_3 + T_4. \tag{A.12}$$

Here the definition of T_1, T_2, T_3, and T_4 respects the order of the four terms in the second to last equality of Equation (A.12). We shall proceed to prove that each T_1, T_2, T_3, T_4 is bounded by the right hand side of Equation (A.8).

For T_1, using the Cauchy–Schwarz inequality, we have

$$
\begin{aligned}
T_1 &= \sum_{K \in \mathcal{T}} \left\langle \varepsilon_{i,\mathcal{J}} u_{i,\mathcal{J}} + \frac{1}{2} \Delta u_{i,\mathcal{J}} - V_{\text{eff}} u_{i,\mathcal{J}}, v - v_{\mathcal{J}} \right\rangle_K \\
&\quad + \sum_{K \in \mathcal{T}} \langle \varepsilon_i u_i - \varepsilon_{i,\mathcal{J}} u_{i,\mathcal{J}} - V_{\text{eff}} u_i + V_{\text{eff}} u_{i,\mathcal{J}}, v - v_{\mathcal{J}} \rangle_K \\
&\leq \sum_{K \in \mathcal{T}} \left\| \varepsilon_{i,\mathcal{J}} u_{i,\mathcal{J}} + \frac{1}{2} \Delta u_{i,\mathcal{J}} - V_{\text{eff}} u_{i,\mathcal{J}} \right\|_K \| v - v_{\mathcal{J}} \|_K \\
&\quad + \sum_{K \in \mathcal{T}} \| \varepsilon_i u_i - \varepsilon_{i,\mathcal{J}} u_{i,\mathcal{J}} - V_{\text{eff}} u_i + V_{\text{eff}} u_{i,\mathcal{J}} \|_K \| v - v_{\mathcal{J}} \|_K \\
&= \sum_{K \in \mathcal{T}} \left(\sqrt{\gamma_1(J_K)} \left\| \varepsilon_{i,\mathcal{J}} u_{i,\mathcal{J}} + \frac{1}{2} \Delta u_{i,\mathcal{J}} - V_{\text{eff}} u_{i,\mathcal{J}} \right\|_K \right) \left(\frac{1}{\sqrt{\gamma_1(J_K)}} \| v - v_{\mathcal{J}} \|_K \right) \\
&\quad + \sum_{K \in \mathcal{T}} \left(\sqrt{\gamma_1(J_K)} \| \varepsilon_i u_i - \varepsilon_{i,\mathcal{J}} u_{i,\mathcal{J}} - V_{\text{eff}} u_i + V_{\text{eff}} u_{i,\mathcal{J}} \|_K \right) \left(\frac{1}{\sqrt{\gamma_1(J_K)}} \| v - v_{\mathcal{J}} \|_K \right).
\end{aligned}
\tag{A.13}
$$

Using Equation (3.1), we obtain

$$
\begin{aligned}
T_1 &\lesssim \sum_{K \in \mathcal{T}} \eta_{i,R_K} \| \nabla v \|_K + \sqrt{\gamma_{1,\mathcal{J}}} \sum_{K \in \mathcal{T}} \xi_{i,K} \| \nabla v \|_K \\
&\lesssim \left(\eta_{i,R} + \sqrt{\gamma_{1,\mathcal{J}}} \xi_i \right) \| v \|_{E,\mathcal{T}}.
\end{aligned}
\tag{A.14}
$$

For T_2, using Equation (3.2), we obtain

$$
\begin{aligned}
T_2 &\lesssim \left(\sum_{F \in \mathcal{S}} \gamma_2(J_F) \alpha^2(J_F) \left\| [\![u_{i,\mathcal{J}}]\!] \right\|_F^2 \right)^{\frac{1}{2}} \left(\sum_{F \in \mathcal{S}} \frac{1}{\gamma_2(J_F)} \left\| [\![v - v_{\mathcal{J}}]\!] \right\|_F^2 \right)^{\frac{1}{2}} \\
&\lesssim \eta_{i,V} \left(\sum_{K \in \mathcal{T}} \frac{1}{\gamma_2(J_K)} \| v - v_{\mathcal{J}} \|_{\partial K}^2 \right)^{\frac{1}{2}} \\
&\lesssim \eta_{i,V} \| v \|_{E,\mathcal{T}}.
\end{aligned}
\tag{A.15}
$$

Similarly, for T_3, we have

$$
\begin{aligned}
T_3 &\lesssim \left(\sum_{F \in \mathcal{S}} \gamma_2(J_F) \left\| [\![\nabla u_{i,\mathcal{J}}]\!] \right\|_F^2 \right)^{\frac{1}{2}} \left(\sum_{F \in \mathcal{S}} \frac{1}{\gamma_2(J_F)} \left\| \{\!\{ v - v_{\mathcal{J}} \}\!\} \right\|_F^2 \right)^{\frac{1}{2}} \\
&\lesssim \eta_{i,G} \left(\sum_{K \in \mathcal{T}} \frac{1}{\gamma_2(J_K)} \| v - v_{\mathcal{J}} \|_{\partial K}^2 \right)^{\frac{1}{2}} \\
&\lesssim \eta_{i,G} \| v \|_{E,\mathcal{T}}.
\end{aligned}
\tag{A.16}
$$

Using the Cauchy–Schwarz inequality and the inverse trace inequality (3.6), we have

$$
T_4 \lesssim \left(\sum_{F \in \mathcal{S}} \gamma_2(J_F) \alpha^2(J_F) \left\| [\![u_{i,\mathcal{J}}]\!] \right\|_F^2 \right)^{\frac{1}{2}} \left(\sum_{F \in \mathcal{S}} \frac{1}{\gamma_2(J_F) \alpha^2(J_F)} \left\| \{\!\{ \nabla v_{\mathcal{J}} \}\!\} \right\|_F^2 \right)^{\frac{1}{2}}
$$
$$
\lesssim \eta_{i,V} \left(\sum_{K \in \mathcal{T}} \left\| \nabla v_{\mathcal{J}} \right\|_K^2 \right)^{\frac{1}{2}}. \tag{A.17}
$$

From Equation (3.3), we have

$$
\sum_{K \in \mathcal{T}} \left\| \nabla v_{\mathcal{J}} \right\|_K^2 \leq \sum_{K \in \mathcal{T}} \left\| \nabla(v - v_{\mathcal{J}}) \right\|_K^2 + \sum_{K \in \mathcal{T}} \left\| \nabla v \right\|_K^2 \lesssim \left\| v \right\|_{E,\mathcal{T}}^2, \tag{A.18}
$$

and therefore

$$
T_4 \lesssim \eta_{i,V} \left\| v \right\|_{E,\mathcal{T}}. \tag{A.19}
$$

Combining equations (A.14), (A.15), (A.16), and (A.19) completes the proof of the lemma.   □

LEMMA A.4.   *If Assumption 3.1 holds, let $(\varepsilon_{i,\mathcal{J}}, u_{i,\mathcal{J}})$ be a computed eigenpair corresponding to (2.20), and let (ε_i, u_i) be an eigenpair corresponding to (2.25). Then for $u_{i,\mathcal{J}}^c = I_{\mathcal{J}} u_{i,\mathcal{J}}$ we have*

$$
\left\| u_i - u_{i,\mathcal{J}}^c \right\|_{E,\mathcal{T}} \lesssim \eta_i + \left(1 + \sqrt{\gamma_{1,\mathcal{J}}}\right) \xi_i. \tag{A.20}
$$

Proof.   Since $v \equiv u_i - u_{i,\mathcal{J}}^c \in H_\pi^1(\Omega)$,

$$
\left\| u_i - u_{i,\mathcal{J}}^c \right\|_{E,\mathcal{T}}^2 = A\left(u_i - u_{i,\mathcal{J}}^c, v \right). \tag{A.21}
$$

Then

$$
\begin{aligned}
A\left(u_i - u_{i,\mathcal{J}}^c, v \right) &= \langle \varepsilon_i u_i - V_{\mathrm{eff}} u_i, v \rangle_\Omega - A(u_{i,\mathcal{J}}^c, v) \\
&= \langle \varepsilon_i u_i - V_{\mathrm{eff}} u_i, v \rangle_\Omega - D_{\mathcal{J}}(u_{i,\mathcal{J}}^c, v) \\
&= \langle \varepsilon_i u_i - V_{\mathrm{eff}} u_i, v \rangle_\Omega - D_{\mathcal{J}}(u_{i,\mathcal{J}}, v) + \frac{1}{2} \sum_{K \in T} \langle \nabla u_{i,\mathcal{J}}^r, \nabla v \rangle_K.
\end{aligned} \tag{A.22}
$$

Using the fact that

$$
\langle \varepsilon_{i,\mathcal{J}} u_{i,\mathcal{J}}, v_{\mathcal{J}} \rangle = D_{\mathcal{J}}(u_{i,\mathcal{J}}, v_{\mathcal{J}}) + K_{\mathcal{J}}(u_{i,\mathcal{J}}, v_{\mathcal{J}}) + \langle V_{\mathrm{eff}} u_{i,\mathcal{J}}, v_{\mathcal{J}} \rangle_{\mathcal{T}}, \tag{A.23}
$$

where $v_{\mathcal{J}}$ is the approximation to v satisfying equations (3.1), (3.2), and (3.3), we have

$$
\begin{aligned}
A\left(u_i - u_{i,\mathcal{J}}^c, v \right) &= \langle \varepsilon_i u_i - V_{\mathrm{eff}} u_i, v_{\mathcal{J}} \rangle_{\mathcal{T}} + \langle \varepsilon_i u_i - V_{\mathrm{eff}} u_i, v - v_{\mathcal{J}} \rangle_{\mathcal{T}} - D_{\mathcal{J}}(u_{i,\mathcal{J}}, v) \\
&\quad + \frac{1}{2} \sum_{K \in T} \langle \nabla u_{i,\mathcal{J}}^r, \nabla v \rangle_K \\
&= \langle \varepsilon_i u_i - \varepsilon_{i,\mathcal{J}} u_{i,\mathcal{J}} - V_{\mathrm{eff}} u_i + V_{\mathrm{eff}} u_{i,\mathcal{J}}, v_{\mathcal{J}} \rangle_{\mathcal{T}} + \langle \varepsilon_i u_i - V_{\mathrm{eff}} u_i, v - v_{\mathcal{J}} \rangle_{\mathcal{T}} \\
&\quad - D_{\mathcal{J}}(u_{i,\mathcal{J}}, v - v_{\mathcal{J}}) + K_{\mathcal{J}}(u_{i,\mathcal{J}}, v_{\mathcal{J}}) + \frac{1}{2} \sum_{K \in T} \langle \nabla u_{i,\mathcal{J}}^r, \nabla v \rangle_K.
\end{aligned} \tag{A.24}
$$

From Lemma A.3,

$$\langle \varepsilon_i u_i - V_{\text{eff}} u_i, v - v_{\mathcal{J}} \rangle_{\mathcal{T}} - D_{\mathcal{J}}(u_{i,\mathcal{J}}, v - v_{\mathcal{J}}) + K_{\mathcal{J}}(u_{i,\mathcal{J}}, v_{\mathcal{J}}) \lesssim \left(\eta_i + \sqrt{\gamma_{1,\mathcal{J}}} \xi_i \right) \| v \|_{E,\mathcal{T}}. \tag{A.25}$$

Also from the Cauchy–Schwarz inequality and Lemma A.1,

$$\sum_{K \in T} \langle \nabla u_{i,\mathcal{J}}^r, \nabla v \rangle_K \lesssim \| u_{i,\mathcal{J}}^r \|_{E,\mathcal{T}} \| v \|_{E,\mathcal{T}} \lesssim \eta_i \| v \|_{E,\mathcal{T}}. \tag{A.26}$$

Finally, defining

$$r_i = \varepsilon_i u_i - \varepsilon_{i,\mathcal{J}} u_{i,\mathcal{J}} - V_{\text{eff}} u_i + V_{\text{eff}} u_{i,\mathcal{J}}, \tag{A.27}$$

we have

$$\langle r_i, v_{\mathcal{J}} \rangle_{\mathcal{T}} = \langle r_i, v_{\mathcal{J}} - \Pi_0 v \rangle_{\mathcal{T}} + \langle r_i, \Pi_0 v \rangle_{\mathcal{T}} = \langle r_i, v_{\mathcal{J}} - \Pi_0 v \rangle_{\mathcal{T}}. \tag{A.28}$$

Here, $\Pi_0 v = \frac{1}{|\Omega|} \int v(\mathbf{r}) d\mathbf{r}$ is a constant and $\langle r_i, \Pi_0 v \rangle_{\mathcal{T}}$ vanishes due to equations (2.13), (2.18), and (2.20). We have

$$\| v_{\mathcal{J}} - \Pi_0 v \|_{\mathcal{T}} \leq \| v_{\mathcal{J}} - v \|_{\mathcal{T}} + \| v - \Pi_0 v \|_{\Omega}. \tag{A.29}$$

Using the Poincaré inequality,

$$\| v - \Pi_0 v \|_{\Omega} \leq C_p \| \nabla v \|_{\Omega} \tag{A.30}$$

where C_p is the Poincaré constant for domain Ω. In the current context, C_p is independent of the choice of basis functions, and we have $C_p \lesssim 1$. Using Equation (3.1), we have

$$\| v_{\mathcal{J}} - \Pi_0 v \|_{\mathcal{T}} \lesssim (\sqrt{\gamma_{1,\mathcal{J}}} + C_p) \| \nabla v \|_{\Omega} \lesssim (1 + \sqrt{\gamma_{1,\mathcal{J}}}) \| v \|_{E,\mathcal{T}}. \tag{A.31}$$

Again, using the Cauchy–Schwarz inequality, we obtain

$$\langle r_i, v_{\mathcal{J}} \rangle_{\mathcal{T}} \lesssim (1 + \sqrt{\gamma_{1,\mathcal{J}}}) \xi_i \| v \|_{E,\mathcal{T}}. \tag{A.32}$$

Lemma A.4 follows directly from equations (A.25), (A.26), and (A.32). □

LEMMA A.5. *For all* $v \in H_\pi^1(\Omega) \oplus \mathcal{V}_{\mathcal{J}}(\mathcal{T})$,

$$\| \mathcal{L} v \|_{\mathcal{T}} \leq C_{\mathcal{J}} \| [\![v]\!] \|_{\mathcal{S}}, \tag{A.33}$$

where the constant $C_{\mathcal{J}}$ *only depends on the function spaces* $\mathcal{V}_{\mathcal{J}}(\mathcal{T})$ *and* $\mathcal{W}_{\mathcal{J}}(\mathcal{T})$ *and is expressed as*

$$C_{\mathcal{J}} = \sup_{\mathbf{q} \in \mathcal{W}_{\mathcal{J}}(\mathcal{T})} \frac{\| \{\!\{ \mathbf{q} \}\!\} \|_{\mathcal{S}}}{\| \mathbf{q} \|_{\mathcal{T}}}. \tag{A.34}$$

Proof. Use the definition of the lifting operator and the Cauchy–Schwarz inequality to obtain

$$\| \mathcal{L} v \|_{\mathcal{T}}^2 = \langle [\![v]\!], \{\!\{ \mathcal{L} v \}\!\} \rangle_{\mathcal{S}} \leq \| [\![v]\!] \|_{\mathcal{S}} \| \{\!\{ \mathcal{L} v \}\!\} \|_{\mathcal{S}}. \tag{A.35}$$

Note that $\mathcal{L}v \in \mathcal{W}_\mathcal{J}(\mathcal{T})$ and

$$\left\| \{\!\{\mathcal{L}v\}\!\} \right\|_\mathcal{S} \leq \left(\sup_{\mathbf{q} \in \mathcal{W}_\mathcal{J}(\mathcal{T})} \frac{\left\| \{\!\{\mathbf{q}\}\!\} \right\|_\mathcal{S}}{\|\mathbf{q}\|_\mathcal{T}} \right) \|\mathcal{L}v\|_\mathcal{T} \equiv C_\mathcal{J} \|\mathcal{L}v\|_\mathcal{T}. \tag{A.36}$$

Since $\mathcal{W}_\mathcal{J}(\mathcal{T})$ is finite dimensional, the constant $C_\mathcal{J}$ defined in Equation (A.34) is finite and only depends on the function spaces $\mathcal{V}_\mathcal{J}(\mathcal{T})$ and $\mathcal{W}_\mathcal{J}(\mathcal{T})$. Then

$$\|\mathcal{L}v\|_\mathcal{T}^2 \leq C_\mathcal{J} \left\| [\![v]\!] \right\|_\mathcal{S} \|\mathcal{L}v\|_\mathcal{T}. \tag{A.37}$$

Eliminating $\|\mathcal{L}v\|_\mathcal{T}$ from both sides of Equation (A.37), we arrive at Equation (A.33). $\square$

LEMMA A.6.   *If the penalty parameter satisfies*

$$\alpha(J_F) > 2C_\mathcal{J}^2 \tag{A.38}$$

for $C_\mathcal{J}$ defined in Equation (A.34), *then for all $u \in H_\pi^1(\Omega) \oplus \mathcal{V}_\mathcal{J}(\mathcal{T})$,*

$$\frac{1}{2} \|u\|_{E,\mathcal{T}}^2 \leq \widetilde{A}_\mathcal{J}(u,u) \leq 2 \|u\|_{E,\mathcal{T}}^2. \tag{A.39}$$

I.e., the extended bilinear form $\widetilde{A}_\mathcal{J}(u,v)$ defined in Equation (3.22) *is both coercive and continuous with respect to the energy norm on $H_\pi^1(\Omega) \oplus \mathcal{V}_\mathcal{J}(\mathcal{T})$.*

Proof.   We first prove the coercivity. Using the Cauchy–Schwarz inequality, we have

$$\begin{aligned}
\widetilde{A}_\mathcal{J}(u,u) &= \frac{1}{2} \langle \nabla u, \nabla u \rangle_\mathcal{T} - \langle \mathcal{L}u, \nabla u \rangle_\mathcal{T} + \sum_{F \in \mathcal{S}} \alpha(J_F) \langle [\![u]\!], [\![u]\!] \rangle_F \\
&\geq \frac{1}{2} \langle \nabla u, \nabla u \rangle_\mathcal{T} - \|\mathcal{L}u\|_\mathcal{T} \|\nabla u\|_\mathcal{T} + \sum_{F \in \mathcal{S}} \alpha(J_F) \langle [\![u]\!], [\![u]\!] \rangle_F \\
&\geq \frac{1}{2} \langle \nabla u, \nabla u \rangle_\mathcal{T} - \frac{1}{2\theta} \langle \mathcal{L}u, \mathcal{L}u \rangle_\mathcal{T} - \frac{\theta}{2} \langle \nabla u, \nabla u \rangle_\mathcal{T} + \sum_{F \in \mathcal{S}} \alpha(J_F) \langle [\![u]\!], [\![u]\!] \rangle_F \\
&\geq \frac{1-\theta}{2} \langle \nabla u, \nabla u \rangle_\mathcal{T} + \sum_{F \in \mathcal{S}} \left(\alpha(J_F) - \frac{C_\mathcal{J}^2}{2\theta} \right) \langle [\![u]\!], [\![u]\!] \rangle_F.
\end{aligned} \tag{A.40}$$

The last inequality in (A.40) uses Lemma A.5, and θ can be any positive constant. Here, we choose $\theta = \frac{1}{2}$. Using the assumption that $\alpha(J_F) > 2C_\mathcal{J}^2$,

$$\widetilde{A}_\mathcal{J}(u,u) \geq \frac{1}{4} \langle \nabla u, \nabla u \rangle_\mathcal{T} + \frac{1}{2} \sum_{F \in \mathcal{S}} \alpha(J_F) \langle [\![u]\!], [\![u]\!] \rangle_F = \frac{1}{2} \|u\|_{E,\mathcal{T}}^2, \tag{A.41}$$

which proves the coercivity of the extended bilinear form.

We apply the same procedure to prove continuity:

$$\begin{aligned}
\widetilde{A}_\mathcal{J}(u,u) &\leq \frac{1}{2} \langle \nabla u, \nabla u \rangle_\mathcal{T} + \|\mathcal{L}u\|_\mathcal{T} \|\nabla u\|_\mathcal{T} + \sum_{F \in \mathcal{S}} \alpha(J_F) \langle [\![u]\!], [\![u]\!] \rangle_F \\
&\leq \frac{1}{2} \langle \nabla u, \nabla u \rangle_\mathcal{T} + \frac{1}{2\theta} \langle \mathcal{L}u, \mathcal{L}u \rangle_\mathcal{T} + \frac{\theta}{2} \langle \nabla u, \nabla u \rangle_\mathcal{T} + \sum_{F \in \mathcal{S}} \alpha(J_F) \langle [\![u]\!], [\![u]\!] \rangle_F
\end{aligned}$$

$$\leq \frac{1+\theta}{2} \langle \nabla u, \nabla u \rangle_{\mathcal{T}} + \sum_{F \in \mathcal{S}} \left(\alpha(J_F) + \frac{C_{\mathcal{J}}^2}{2\theta} \right) \langle [\![u]\!], [\![u]\!] \rangle_F. \tag{A.42}$$

Again, θ can be any positive constant. Here, we choose $\theta = 1$. Then,

$$\widetilde{A}_{\mathcal{J}}(u, u) \leq \langle \nabla u, \nabla u \rangle_{\mathcal{T}} + 2 \sum_{F \in \mathcal{S}} \alpha(J_F) \langle [\![u]\!], [\![u]\!] \rangle_F = 2 \|u\|_{E,\mathcal{T}}^2, \tag{A.43}$$

which proves the continuity of the extended bilinear form. $\qquad\square$

COROLLARY A.7.   *If Equation (A.38) is satisfied, then for $u_{\mathcal{J}} \in \mathcal{V}_{\mathcal{J}}(\mathcal{T})$, we have*

$$\frac{1}{2} \|u_{\mathcal{J}}\|_{E,\mathcal{T}}^2 \leq A_{\mathcal{J}}(u_{\mathcal{J}}, u_{\mathcal{J}}) \leq 2 \|u_{\mathcal{J}}\|_{E,\mathcal{T}}^2. \tag{A.44}$$

I.e., the bilinear form $A_{\mathcal{J}}(u_{\mathcal{J}}, v_{\mathcal{J}})$ is both coercive and continuous with respect to the energy norm on $\mathcal{V}_{\mathcal{J}}(\mathcal{T})$.

Proof.   Just note that $\widetilde{A}(u_{\mathcal{J}}, v_{\mathcal{J}}) = A_{\mathcal{J}}(u_{\mathcal{J}}, v_{\mathcal{J}})$ for $u_{\mathcal{J}}, v_{\mathcal{J}} \in \mathcal{V}_{\mathcal{J}}(\mathcal{T})$ and use Lemma A.6. $\qquad\square$

LEMMA A.8.   *Let $(\varepsilon_{i,\mathcal{J}}, u_{i,\mathcal{J}})$ be a computed eigenpair corresponding to (2.20), and let (ε_i, u_i) be an eigenpair corresponding to (2.13). Then we have the following identities:*

$$\widetilde{A}_{\mathcal{J}}(u_i - u_{i,\mathcal{J}}, u_i - u_{i,\mathcal{J}}) + \langle V_{\mathrm{eff}}(u_i - u_{i,\mathcal{J}}), (u_i - u_{i,\mathcal{J}}) \rangle_{\mathcal{T}}$$
$$= \varepsilon_i \|u_i - u_{i,\mathcal{J}}\|_{\Omega}^2 + (\varepsilon_{i,\mathcal{J}} - \varepsilon_i) \|u_{i,\mathcal{J}}\|_{\mathcal{T}}^2 + 2\mathrm{Re}\mathcal{R}(u_i, u_i - u_{i,\mathcal{J}}), \tag{A.45}$$

and

$$\widetilde{A}_{\mathcal{J}}(u_i - u_{i,\mathcal{J}}, u_i - u_{i,\mathcal{J}}) + \langle V_{\mathrm{eff}}(u_i - u_{i,\mathcal{J}}), (u_i - u_{i,\mathcal{J}}) \rangle_{\mathcal{T}}$$
$$= \varepsilon_{i,\mathcal{J}} \|u_i - u_{i,\mathcal{J}}\|_{\Omega}^2 + (\varepsilon_i - \varepsilon_{i,\mathcal{J}}) \|u_i\|_{\Omega}^2 + 2\mathrm{Re}\mathcal{R}_{\mathcal{J}}(u_{i,\mathcal{J}}, u_{i,\mathcal{J}} - u_i). \tag{A.46}$$

Here the extended residuals $\mathcal{R}$ and $\mathcal{R}_{\mathcal{J}}$ are defined in Equation (3.25) and (3.26), respectively.

Proof.   We first prove Equation (A.45):

$$\widetilde{A}_{\mathcal{J}}(u_i - u_{i,\mathcal{J}}, u_i - u_{i,\mathcal{J}}) + \langle V_{\mathrm{eff}}(u_i - u_{i,\mathcal{J}}), (u_i - u_{i,\mathcal{J}}) \rangle_{\mathcal{T}}$$
$$= \varepsilon_i \|u_i\|_{\Omega}^2 + \varepsilon_{i,\mathcal{J}} \|u_{i,\mathcal{J}}\|_{\mathcal{T}}^2 - 2\mathrm{Re}\widetilde{A}_{\mathcal{J}}(u_i, u_{i,\mathcal{J}}) - 2\mathrm{Re}\langle V_{\mathrm{eff}}u_i, u_{i,\mathcal{J}} \rangle_{\mathcal{T}}. \tag{A.47}$$

We have

$$2\mathrm{Re}\widetilde{A}_{\mathcal{J}}(u_i, u_{i,\mathcal{J}}) + 2\mathrm{Re}\langle V_{\mathrm{eff}}u_i, u_{i,\mathcal{J}} \rangle_{\mathcal{T}}$$
$$= 2\mathrm{Re}\widetilde{A}_{\mathcal{J}}(u_i, u_{i,\mathcal{J}} - u_i) + 2\mathrm{Re}\langle V_{\mathrm{eff}}u_i, u_{i,\mathcal{J}} - u_i \rangle_{\mathcal{T}} + 2\mathrm{Re}\widetilde{A}_{\mathcal{J}}(u_i, u_i) + 2\mathrm{Re}\langle V_{\mathrm{eff}}u_i, u_i \rangle_{\mathcal{T}}$$
$$= 2\mathrm{Re}\mathcal{R}(u_i, u_{i,\mathcal{J}} - u_i) + 2\varepsilon_i\mathrm{Re}\langle u_i, u_{i,\mathcal{J}} - u_i \rangle_{\mathcal{T}} + 2\varepsilon_i \langle u_i, u_i \rangle_{\Omega}$$
$$= 2\mathrm{Re}\mathcal{R}(u_i, u_{i,\mathcal{J}} - u_i) + 2\varepsilon_i\mathrm{Re}\langle u_i, u_{i,\mathcal{J}} \rangle_{\mathcal{T}}. \tag{A.48}$$

Moreover,

$$\|u_i - u_{i,\mathcal{J}}\|_{\mathcal{T}}^2 = \|u_i\|_{\Omega}^2 + \|u_{i,\mathcal{J}}\|_{\mathcal{T}}^2 - 2\mathrm{Re}\langle u_i, u_{i,\mathcal{J}} \rangle_{\mathcal{T}}. \tag{A.49}$$

Applying equations (A.48) and (A.49) to Equation (A.47) proves Equation (A.45). Exchanging the role of u_i and $u_{i,\mathcal{J}}$, as well as that of ε_i and $\varepsilon_{i,\mathcal{J}}$, in the above derivation gives Equation (A.46). $\qquad\square$

REFERENCES

[1] O.K. Andersen and T. Saha-Dasgupta, *Muffin-tin orbitals of arbitrary order*, Phys. Rev. B, 62, R16219–R16222, 2000.

[2] D.N. Arnold, *An interior penalty finite element method with discontinuous elements*, SIAM J. Numer. Anal., 19, 742–760, 1982.

[3] D.N. Arnold, F. Brezzi, B. Cockburn, and L.D. Marini, *Unified analysis of discontinuous Galerkin methods for elliptic problems*, SIAM J. Numer. Anal., 39, 1749–1779, 2002.

[4] I. Babuška and M. Zlámal, *Nonconforming elements in the finite element method with penalty*, SIAM J. Numer. Anal., 10, 863–875, 1973.

[5] R. Becker and R. Rannacher, *An optimal control approach to a posteriori error estimation in finite element methods*, Acta Numer., 10, 1–102, 2001.

[6] V. Blum, R. Gehrke, F. Hanke, P. Havu, V. Havu, X. Ren, K. Reuter, and M. Scheffler, *Ab initio molecular simulations with numeric atom-centered orbitals*, Comput. Phys. Commun., 180, 2175–2196, 2009.

[7] D. Braess, V. Pillwein, and J. Schöberl, *Equilibrated residual error estimates are p-robust*, Comput. Meth. Appl. Mech. Engrg., 198, 1189–1197, 2009.

[8] D.M. Ceperley and B.J. Alder, *Ground state of the electron gas by a stochastic method*, Phys. Rev. Lett., 45, 566–569, 1980.

[9] J. Chelikowsky, N. Troullier, and Y. Saad, *Finite-difference-pseudopotential method: Electronic structure calculations without a basis*, Phys. Rev. Lett., 72, 1240–1243, 1994.

[10] H. Chen, X. Dai, X. Gong, L. He, and A. Zhou, *Adaptive finite element approximations for Kohn–Sham models*, Multiscale Model. Simul., 12(4), 1828–1869, 2014.

[11] M. Chen, G.C. Guo, and L. He, *Systematically improvable optimized atomic basis sets for ab initio calculations*, J. Phys.: Condens. Matter, 22, 445501–445509, 2010.

[12] B. Cockburn, G.E. Karniadakis, and C.-W. Shu, *Discontinuous Galerkin Methods: Theory, Computation and Applications*, Lecture Notes in Computational Science and Engineering, Springer-Verlag, Berlin, 11, 2000.

[13] B. Cockburn and C.-W. Shu, *Runge–Kutta discontinuous Galerkin methods for convection-dominated problems*, J. Sci. Comput., 16, 173–261, 2001.

[14] X. Dai, X. Gong, Z. Yang, D. Zhang, and A. Zhou, *Finite volume discretizations for eigenvalue problems with applications to electronic structure calculations*, Multiscale Model. Sim., 9, 208–240, 2011.

[15] X. Dai, J. Xu, and A. Zhou, *Convergence and optimal complexity of adaptive finite element eigenvalue computations*, Numer. Math., 110, 313–355, 2008.

[16] R.G. Durán, C. Padra, and R. Rodríguez, *A posteriori error estimates for the finite element approximation of eigenvalue problems*, Math. Mod. Meth. Appl. Sci., 13, 1219–1229, 2003.

[17] A. Ern, S. Nicaise, and M. Vohralík, *An accurate H (div) flux reconstruction for discontinuous Galerkin approximations of elliptic problems*, C.R. Math. Acad. Sci. Paris, 345, 709–712, 2007.

[18] S. Giani, *An a posteriori error estimator for hp-adaptive discontinuous Galerkin methods for computing band gaps in photonic crystals*, J. Comput. Appl. Math., 236, 4810–4826, 2012.

[19] S. Giani and E.J.C. Hall, *An a posteriori error estimator for hp-adaptive discontinuous Galerkin methods for elliptic eigenvalue problems*, Math. Mod. Meth. Appl. Sci., 22, 1250030–1250064, 2012.

[20] X. Gonze, B. Amadon, P.M. Anglade, J.M. Beuken, F. Bottin, P. Boulanger, F. Bruneval, D. Caliste, R. Caracas, M. Cote, et al., *Abinit: First-principles approach to material and nanosystem properties*, Comput. Phys. Commun., 180, 2582–2615, 2009.

[21] C. Hartwigsen, S. Goedecker, and J. Hutter, *Relativistic separable dual-space gaussian pseudopotentials from h to rn*, Phys. Rev. B, 58, 3641–3662, 1998.

[22] P. Hohenberg and W. Kohn, *Inhomogeneous electron gas*, Phys. Rev., 136, B864–B871, 1964.

[23] P. Houston, D. Schötzau, and T.P. Wihler, *Energy norm a posteriori error estimation of hp-adaptive discontinuous Galerkin methods for elliptic problems*, Math. Mod. Meth. Appl. Sci., 17, 33–62, 2007.

[24] J. Junquera, O. Paz, and D. Sanchez-Portal, and E. Artacho, *Numerical atomic orbitals for linear-scaling calculations*, Phys. Rev. B, 64, 235111–235119, 2001.

[25] O.A. Karakashian and F. Pascal, *A posteriori error estimates for a discontinuous Galerkin approximation of second-order elliptic problems*, SIAM J. Numer. Anal., 41, 2374–2399, 2003.

[26] W. Kohn and L. Sham, *Self-consistent equations including exchange and correlation effects*, Phys. Rev., 140, A1133–A1138, 1965.

[27] M.G. Larson, *A posteriori and a priori error analysis for finite element approximations of self-adjoint elliptic eigenvalue problems*, SIAM J. Numer. Anal., 38, 608–625, 2000.

[28] L. Lin, J. Lu, L. Ying, and W. E, *Adaptive local basis set for Kohn–Sham density functional theory in a discontinuous Galerkin framework I: Total energy calculation*, J. Comput. Phys., 231, 2140–2154, 2012.

[29] R. Luce and B.I. Wohlmuth, *A local a posteriori error estimator based on equilibrated fluxes*, SIAM J. Numer. Anal., 42, 1394–1414, 2004.

[30] R. Martin, *Electronic Structure — Basic Theory and Practical Methods*, Cambridge Univ. Pr., West Nyack, NY, 2004.

[31] T. Ozaki, *Variationally optimized atomic orbitals for large-scale electronic structures*, Phys. Rev. B, 67, 155108–155112, 2003.

[32] J.E. Pask and P.A. Sterne, *Real-space formulation of the electrostatic potential and total energy of solids*, Phys. Rev. B, 71, 113101–113104, 2005.

[33] M.C. Payne, M.P. Teter, D.C. Allen, T.A. Arias, and J.D. Joannopoulos, *Iterative minimization techniques for ab initio total energy calculation: molecular dynamics and conjugate gradients*, Rev. Mod. Phys., 64, 1045–1097, 1992.

[34] J.P. Perdew and A. Zunger, *Self-interaction correction to density-functional approximations for many-electron systems*, Phys. Rev. B, 23, 5048–5079, 1981.

[35] X. Qian, J. Li, L. Qi, C.Z. Wang, T.L. Chan, Y.X. Yao, K.M. Ho, and S. Yip, *Quasiatomic orbitals for ab initio tight-binding analysis*, Phys. Rev. B, 78, 245112–245134, 2008.

[36] S.I. Repin, *A posteriori estimates for partial differential equations*, Radon Series on Computational and Applied Mathematics, Walter de Gruyter GmbH & Co. KG, Berlin, 4, 2008.

[37] D. Schötzau and L. Zhu, *A robust a posteriori error estimator for discontinuous Galerkin methods for convection–diffusion equations*, Appl. Numer. Math., 59, 2236–2255, 2009.

[38] B. Stamm and T. Wihler, *hp-Optimal discontinuous Galerkin methods for linear elliptic problems*, Math. Comput., 79, 2117–2133, 2010.

[39] N. Troullier and J.L. Martins, *Efficient pseudopotentials for plane-wave calculations*, Phys. Rev. B, 43, 1993–2006, 1991.

[40] E. Tsuchida and M. Tsukada, *Electronic-structure calculations based on the finite-element method*, Phys. Rev. B, 52, 5573–5578, 1995.

[41] R. Verfürth, *A Review of A Posteriori Error Estimation and Adaptive Mesh-Refinement Techniques*, Wiley-Teubner, New York, 1996.

[42] A. Warshel and M. Levitt, *Theoretical studies of enzymic reactions: dielectric, electrostatic and steric stabilization of the carbonium ion in the reaction of lysozyme*, J. Mol. Biol., 103, 227–249, 1976.

[43] M.F. Wheeler, *An elliptic collocation-finite element method with interior penalties*, SIAM J. Numer. Anal., 15, 152–161, 1978.

[44] Z. Zhao, J. Meza, and L.W. Wang, *A divide-and-conquer linear scaling three-dimensional fragment method for large scale electronic structure calculations*, J. Phys. Condens. Matter, 20, 294203–294210, 2008.